



A State-of-the-Art Review of Crack Branching

Yanan Sun^a, Michael G Edwards^a, Bin Chen^b, Chenfeng Li^{a,c,*}

^aZienkiewicz Centre for Computational Engineering, College of Engineering, Swansea University Bay Campus, Swansea SA1 8EN, United Kingdom

^bLawrence Berkeley National Laboratory, Berkeley, CA 94720, United States

^cEnergy Safety Research Institute, College of Engineering, Swansea University Bay Campus, Swansea SA1 8EN, United Kingdom

Abstract

Crack branching has important theoretical and practical significance in many natural phenomena and practical engineering problems. At present, the field of crack branching is still at an exploration stage, lacking a unified explanation of the underlying mechanisms and an effective method to predict crack branching in practical materials. This paper provides a state-of-the-art review of crack branching, including experimental observations, physics, fracture models and associated numerical methods. The experimental observations are first summarized, followed by the physics of crack branching. Then, the crack models including discrete crack models and smeared crack models are discussed, highlighting their key features, advantages and limitations. Next, a number of numerical methods that have been used to simulate crack branching are reviewed in detail, including the finite element method (FEM), extended finite element method (XFEM), boundary element method (BEM), meshfree methods (MMs), peridynamics (PD) and discrete element method (DEM). Finally, based on the information reviewed above, the future research directions of crack branching modelling are discussed.

Keywords: crack branching; fracture propagation; experiment; criterion; numerical simulation

1. Introduction

Crack branching is encountered in many practical engineering problems, and is particularly common in brittle materials and metal alloys with stress corrosion cracking [1, 2]. As shown in Fig. 1, crack branching can occur symmetrically or asymmetrically. The study of crack branching phenomena, including branching mechanisms, branching criteria, experimental measurement and numerical simulation, is of great significance for robust and reliable prediction of crack propagation. A good understanding of the initiation and propagation of cracks inside structural materials is important for preventing catastrophic failure of engineering components and for developing new materials.

The theory of straight line crack expansion is basically mature, with the help of three main types of investigation techniques, namely experimental, analytical and numerical techniques. The mechanism for crack propagation is examined using the simple energy balance theory: the crack occurs when the energy available for crack growth is sufficient to overcome the resistance of the material [5]. In linear elastic fracture mechanics, the propagation criteria of a single steady crack are mainly based on the concept of stress intensity factor or energy release rate. While in nonlinear fracture mechanics, the J -integral is often applied, which can be viewed as a nonlinear stress intensity parameter or energy release rate. However, the mechanism for crack branching is more complex and still in exploration. The propagation velocity was thought to be a determining factor in crack branching: when the crack

*Corresponding author: c.f.li@swansea.ac.uk

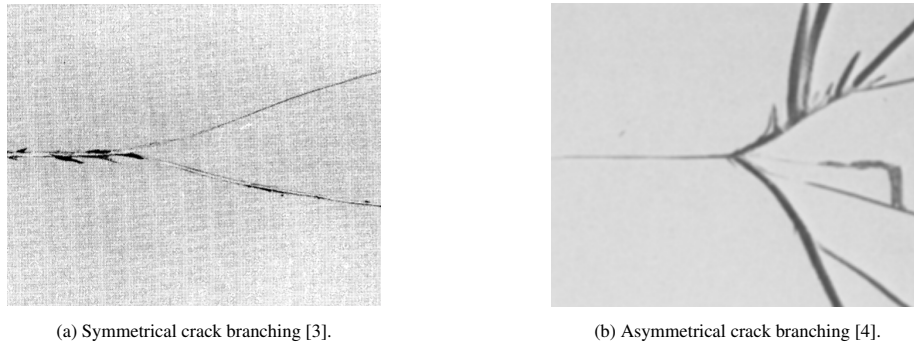


Figure 1: Crack branching photographs from experimental results.

24 velocity exceeds the critical value, the stress field in front of the crack tip changes and branching occurs. However, it
 25 was later found that experimentally observed crack velocities at crack branches were much smaller than the theoretical
 26 ones [3]. Therefore, other mechanisms were considered, including the existence of microcracks, tilting and twisting
 27 of the stress vector at the crack front and dynamic instabilities. If near-tip instabilities are suppressed, then supersonic
 28 cracks are also possible [6]. While many studies on the crack branching phenomenon have been performed both
 29 experimentally and theoretically, a uniform theory that accounts for dynamic crack propagation instability and crack
 30 branching remains an open question.

31 In addition to the experimental and analytical techniques, numerical simulations are also employed to study crack
 32 branching. Various crack models and numerical methods have been proposed to simulate crack initiation and propa-
 33 gation including crack branching and intersection with reasonable computational cost, and both crack propagation
 34 velocity and branching angles have been correctly predicted. With the development of numerical techniques, the
 35 modelling of complex crack propagation processes has become more accurate and robust, while the mechanism of
 36 crack branching has been further understood. Crack models essentially divide into two categories: discrete crack
 37 models and smeared crack models. Popular discrete crack models usually represent the fracture topology explicitly,
 38 which include remeshing, element deletion, enrichment, cracking particles, and cohesive zone models. Smeared crack
 39 models average the crack over a certain width without explicit tracking of fracture surfaces, and they include nonlocal
 40 models, gradient models, viscous models and phase field models. Based on whether spatial derivatives are employed
 41 in the controlling equation, the main numerical methods for crack branching can also be summarized in two cate-
 42 gories: continuum methods and discontinuum methods. The continuum methods model the domain as a continuous
 43 body and use partial differential equations with spatial derivatives to describe the underlying physics. They include
 44 the finite element method (FEM), the extended finite element method (XFEM), the boundary element method (BEM),
 45 and the meshfree methods (MMs). Spatial derivatives are avoided in the discontinuum methods. The peridynamic
 46 method (PD) and the discrete element method (DEM) are two commonly used discontinuum methods. Each numeri-
 47 cal method has its advantages and disadvantages, and no consensus has been reached on a standard general numerical
 48 simulator for crack branching.

49 While dynamic crack propagation has been investigated in the literature [7, 8], there has been little effort to
 50 systematically examine crack branching. Therefore, the aim of this work is to summarize the research on crack
 51 branching and lead to an improved understanding of branching mechanisms and the study direction in the future. The
 52 structure of the paper is arranged as follows. The experimental results on crack branching are summarized in § 2.
 53 Based on the experimental results as well as the theoretical derivations, the physics of crack branching is provided in
 54 § 3, which includes § 3.1 describing the causes of crack branching and § 3.2 describing commonly used branching
 55 criteria. § 4 summarises and compares different crack models and numerical methods for crack branching. Finally,
 56 § 5 summarises the existing findings related to crack branching, highlights some of the most demanding outstanding
 57 questions, and indicates potential directions for future research.

Nomenclature	
$a_0 - a_7$	parameters in the Newmark method
A	area
\mathbf{b}	prescribed body-force density field
c	peridynamic material parameter
c_d	cohesion
c_R	Rayleigh wave speed
c_S	shear wave speed
$E(\mathbf{u}, \Gamma)$	energy functional
$E_\epsilon(\mathbf{u}, \Gamma)$	regularized energy functional
$f(\phi)$	energetic degradation function in phase field models
\mathbf{f}	pairwise force in peridynamics
F_n, F_s	normal force and shear force
F_{lm}	dimensionless function of the branching angle coefficient when branching velocity tends to zero
$\{\mathbf{F}\}$	global vector of nodal load
$g_1(v)$	decreasing function of the crack velocity
G, G'	energy release rate before and after branching
G^{dyn}	dynamic energy release rate
G_c	fracture toughness
\mathcal{H}	horizon in peridynamics
H_{lm}	dimensionless function of the branching angle coefficient and crack velocity before and after branching
$H(\mathbf{x})$	Heaviside function
$J(\mathbf{x})$	junction function
$k(v), k_I(v')$	function of crack velocity and branching velocity
k_n, k_s	normal stiffness and shear stiffness
K_c	initial stiffness in the intrinsic cohesive zone model
K_I, K_I^{dyn}	stress intensity factor and dynamic stress intensity factor
K_I^0	instantaneous stress intensity factor
K_{Ib}	critical branching stress intensity factor
K_{ID}	dynamic crack growth toughness
K'_I	dynamic stress intensity factor after branching
K_{0m}	rest stress intensity factor before branching
\mathbf{K}	stiffness matrix
l	crack length
l_0	length scale
\mathbf{M}	mass matrix
N, N_c	set of all nodes and cracked nodes
\hat{N}_i, N_i	continuous shape function and discontinuous shape function
N^H, N^T, N^J	set of nodes to enrich for the crack, the crack tip and the junction
\mathbf{q}_i	additional degrees of freedom in cracking particles methods
r_c, r_0	characteristic distance and instantaneous characteristic distance
s	stretch of the bond
S	sign function defined as 1 and -1 on two sides of the crack
t	time
\mathbf{t}	traction
\mathbf{T}_c	cohesive traction
\mathbf{T}_{ij}	fundamental solutions for traction
\mathbf{T}_{max}	cohesive strength of the material
u_n	normal displacement
$\mathbf{u}, \dot{\mathbf{u}}, \ddot{\mathbf{u}}$	displacement vector, velocity vector, and acceleration vector
$\{\mathbf{u}\}, \{\dot{\mathbf{u}}\}, \{\ddot{\mathbf{u}}\}$	global vectors of nodal displacement, nodal velocity and nodal acceleration
$[[\mathbf{u}]]$	displacement jump
\mathbf{u}^h	displacement approximation
\mathbf{U}_{ij}	fundamental solutions for displacement
v, v'	crack velocity and branching velocity
v_c	critical crack velocity

Nomenclature	
V volume of a material point	Γ crack set, or sharp crack surface
w crack opening	Γ_n^+, Γ_n^- upper and lower crack surfaces
w_{max} maximum crack opening	Γ_S the outer boundary
\mathbf{x}, \mathbf{x}' position vectors of point \mathbf{x} and \mathbf{x}' in initial configuration	$\epsilon(\mathbf{u})$ the strain field
\mathbf{X} interior point in the boundary element method	λ branching angle coefficient
\mathbf{y}, \mathbf{y}' position vectors of point \mathbf{x} and \mathbf{x}' in deformed configuration	ρ mass density
$\alpha_j, \alpha_k^\alpha, \alpha_m$ nodal enriched degrees of freedom	ϕ damage-like crack phase-field parameter
β joint friction angle	Φ_α near tip asymptotic field function
γ, γ' fracture energy before and after branching	Ψ elastic energy density
	Ω a domain describing a cracked solid

2. Experimental Observations of Crack Branching

A number of experimental studies on dynamic crack propagation have been carried out to provide qualitative observations and quantitative data for the explanation of crack branching phenomena. In this section, the important experimental results are reviewed in chronological order and wherever applicable these experiments are summarized: (1) from the observation and measurement techniques, for example, the high speed photography and electronic timer; (2) from the experimental material, which includes inorganic glass, Plexiglas, Homalite-100; (3) with respect to loading conditions such as dynamic loading and quasi-static loading; (4) from the research objectives, including the conditions under which crack branching occurs (crack tip speed, stress intensity factor and its rate) and how crack propagation proceeds after branching (e.g. the branching angle).

Schardin [9] performed pioneering work on observing crack branching in inorganic glasses with a multiple spark camera technique and noted that the crack speed remains at a constant value when crack bifurcation occurs. A significant decrease of crack speed only occurs when hackle marks appear as a result of surface energy increase. The number of crack branches greatly increases when increasing loading stress. Kerkhof [10] produced predictable crack surface undulation by imposing stress waves with ultrasonic transducers to measure the crack speed and proposed that the limiting velocity is highly related to the composition of inorganic glass. Kobayashi and Mall [11] and Dally [12] determined the dynamic fracture toughness of Homalite-100 and crack propagation velocity variation with dynamic photoelasticity. Dally [12] further modified the equation describing the relationship between the number of branches, the arrest toughness and branching toughness based on the experiment data. The number of branches is in proportion to the ratio of branching toughness to arrest toughness. Ravi-Chandar and Knauss [13, 14, 4, 15] examined the dynamic crack propagation and branching problem in Homalite-100 comprehensively using high speed photomicrography with the load triggered by an electrical pulse. A series of important conclusions were obtained: (1) the stress intensity factor increases while crack velocity remains constant, and there exists a quantitative correlation between the stress intensity factor and the fracture surface roughness (mirror, mist and hackle); (2) from macroscopic examination of the fracture surface, it is found that a crack dissipates excess energy supplied to the crack tip by creating a rough surface rather than by changing the velocity of crack propagation; (3) from microscopic observations of fracture surface roughness, it is found that crack branching is a natural evolution from a “cloud” of microcracks that accompany and lead the main crack; (4) The terminal velocity in Homalite-100 was found to be $0.45c_R$, about half of the Rayleigh wave speed c_R .

Following the work by Ravi-Chandar and Knauss [13, 14, 4, 15], Fineberg et al. [16, 17], Sharon et al. [18], Sharon and Fineberg [19], Sharon et al. [20] investigated the micro-branch instabilities with a series of experiments performed on thin sheets of Plexiglas (PMMA). Fineberg et al. [16] designed an experimental system where the resistance voltage increases as a crack progresses across a sample and cuts the conductive layer, the crack velocity is measured

89 by detecting the voltage. By plotting the evolution of crack velocity during crack growth, the existence of dynamic
 90 instabilities in a brittle fracture is detected. Fineberg et al. [17] found that once the crack velocity is greater than a
 91 critical value, dynamic instabilities occur and the amplitude of the oscillations depends linearly on the mean velocity
 92 of the crack. To explain the origin of instability, Sharon et al. [18] investigated the presence of microscopic local crack
 93 branching as a possible source for instability in dynamic fractures occurring in thin sheets of brittle PMMA. The crack
 94 micro-branches are observed and measured optically and a connection between microscopic and macroscopic crack
 95 branching is established. Later, with the same experiment system, Sharon et al. [20] measured both the energy flux
 96 into the tip of a moving crack and the total surface area created via the microbranching instability. It is found that
 97 a crack does not need to dissipate increasing amounts of energy by accelerating because it has another option of
 98 dissipating energy by creating an increased fracture surface, which provides an explanation for why the theoretical
 99 limiting velocity of a crack is never realized. Readers are referred to [21] for a comprehensive review of the early
 100 work on the micro-branching instability. In recent years, under the help of brittle poly-acrylamide gel (an aqueous
 101 elastomer), which enables probing the fracture process in unprecedented detail by high-speed cameras, a number
 102 of important experiments have been carried out to study the dynamic fracture process [22, 23, 24, 25]. Fineberg
 103 and Bouchbinder [26] reviewed these experimental developments. It has been shown that (1) an intrinsic length
 104 scale, which is associated with nonlinear elastic deformation near the crack tip, plays an important role in dynamic
 105 instabilities; (2) dynamic instabilities include micro-branching instabilities and oscillatory instabilities. The micro-
 106 branching instability may be closely related to the oscillatory instability and it appears to be an intrinsically 3D
 107 instability instead of a 2D instability. Further discussions about the physics of crack branching can be found in § 3.1.

108 A necessary and sufficient condition for crack branching was proposed by Ramulu and Kobayashi [3] (see further
 109 discussions in § 3.2). Hawong et al. [27] verified the criteria by using the 16-spark-gap camera to record the dynamic
 110 photoelastic patterns of curving and branching cracks in Homalite-100 specimens under biaxial loading conditions.
 111 Increasing the biaxial stress ratio of horizontal loading to vertical loading and the stress level increases both the
 112 curvature and the number of branching cracks. Hauch and Marder [28] investigated the modes of energy dissipation
 113 in dynamic crack propagation and branching process in Homalite-100 by using a potential drop technique and made
 114 qualitative comparisons with PMMA. Suzuki et al. [29] investigated fast-growing cracks before and after bifurcation
 115 by using high-speed holographic microscopy and obtained the crack branching velocity, branching angles, and energy
 116 release rate in Homalite 100 and Araldite B. In Homalite 100 the crack branching velocity is $0.48C_R$ with an average
 117 branching angle of $17 \pm 6^\circ$, and in Araldite B the crack branching velocity is $0.46C_R$ with an average branching
 118 angle of $16 \pm 4^\circ$. The energy release rate increases gradually and continuously across the bifurcation point both in
 119 Homalite 100 and in Araldite B and PMMA. Murphy et al. [30] observed the branching patterns of PMMA single edge
 120 notched tensile specimens with scanning electron and optical microscopes and measured the crack propagation speed
 121 by electrical resistance methods. Each macroscopic branch is accompanied by many small cracks along its length with
 122 most crack branches being straight. The experimental results indicate that crack branching is a natural outcome of
 123 the growth and coalescence with microcracks. Both subsurface damage and the frequency of crack speed oscillations
 124 increase during the branching process. Fayyad and Lees [31] gave an example of using digital image correlation
 125 (DIC) to investigate the cracking process and branching mechanisms in lightly reinforced concrete beams. The DIC
 126 can visualise surface displacement by tracking the deformation of a random speckle pattern applied to the surface
 127 through digital images acquired at different instances of deformation [32]. Crack branching angles and propagation
 128 path are found to be related to the beam height and ductility. Another technique, called digital gradient sensing
 129 (DGS), employs 2D DIC with an elasto-optic effect to directly quantify both crack-tip fields and crack speeds. Using
 130 this technique, Sundaram and Tippur [33] investigated the branching phenomenon in soda-lime glass and proposed
 131 that the critical material length scale can be a criterion for crack branching. This study overcomes measurement
 132 challenges such as low fracture toughness and high crack propagation speed. Compared with normal observation and
 133 measurement techniques, the DIC and DGS have advantages of lower cost and simpler operation.

134 The advantages and disadvantages of different observation and measurement techniques are summarised in Ta-
 135 ble. 1. In order to better explore the mechanism of crack propagation and branching, current research on experimental
 136 methods is focused on both the improvement of experimental technologies to overcome existing shortcomings and
 137 the development of new experimental technologies. With respect to testing materials, most experiments have adopted
 138 inorganic glass, Plexiglas, and Homalite-100. The limiting velocity is studied in different materials and it is found
 139 that the limiting velocity is $0.5 \sim 0.65c_R$ for glass, $0.6 \sim 0.7c_R$ for PMMA and $0.35 \sim 0.45c_R$ for Homalite-100 [34].
 140 The branching angles are also investigated although they are easily influenced by the loading conditions, geometry

141 and material properties. From a macroscopic viewpoint, the angle subtended by the new branch (immediately after
 142 branching) and the original crack plane typically lies between 10° and 45° [35]. For different materials, detailed ex-
 143 perimental results on branching angles can be found in [21, 35, 36]. The branch shape and branch number are also
 144 influenced by the loading conditions, geometry and material properties. The increasing of loading stress may lead to
 145 the increasing of branch number of the cracks while the loading conditions, geometry and material properties may
 146 have an impact on the branching angle as well as the branch curvature, thus, the branching shape.

Table 1: Experimental techniques for crack branching.

	Techniques	Advantages	Disadvantages
High Speed Photography	(photoelasticity [11, 12], caustics [37], holographic microscopy [29, 38])	high temporal and spatial resolution	high cost
	(DIC [32], DGS [33])	high resolution, low cost, simple experimental setup	low measurement accuracy in stress concentrations (DIC)
Wallner Lines (stress wave fractography [39])		accurate measurement for crack speed	low spatial resolution
Electrical Resistance Methods [30, 40]		high spatial resolution	sensitive to the variation of film thickness

147 3. Physics of Crack Branching

148 3.1. Causes of Crack Branching

149 Many attempts have been made to explain the crack branching phenomenon. One of the classical theories is
 150 from Yoffe [41]. On the assumption that the crack propagates along the direction normal to the maximum stress,
 151 when the velocity is lower than the critical velocity $0.6c_S$, where c_S is the shear wave speed, the crack propagation
 152 process remains at a steady state. When the crack velocity exceeds this critical value, the propagation process becomes
 153 unstable. The stress state at the crack tip will change, and the hoop stress in the vicinity of the crack tip will have a
 154 maximum angle of about 60° from the propagation direction, which may lead to crack branching, as shown in Fig. 2.
 155 By considering a crack growing from zero initial length at a uniform velocity rather than staying constant length,
 156 Broberg [42] further improved Yoffee’s analytical model and reaffirmed that crack branching occurs if the velocity
 157 exceeds $0.6c_S$. The aforementioned studies suggest that the crack propagation become unstable and cracks are more
 158 likely to start branching when the velocity exceeds a critical value. This mechanism is corresponding to the “velocity
 159 criterion”, see details in § 3.2.1. Though this mechanism is not sufficient to explain the branching phenomenon, the
 160 velocity criterion resulted from it is often employed in numerical simulation due to its simplicity.

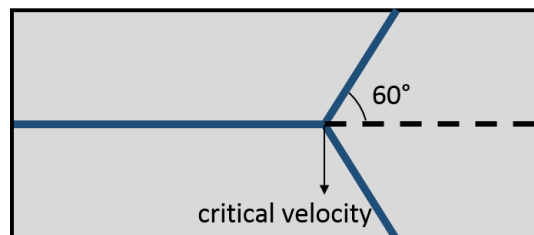


Figure 2: Yoffe’s crack branching model [41].

161 An alternate attempt to explain crack branching is via the viewpoint of energy. By assuming the energy inputting
 162 into the crack and the energy required to create new branch surfaces is balanced, Eshelby [43] argued that the crack tip
 163 velocity should at least be $0.5c_R$ to allow the energy at the crack tip to be sufficient enough to create new surfaces for
 164 crack branches, where c_R is the Rayleigh wave speed. However, according to the experimental observations, the crack
 165 velocity does not change significantly before and after crack branching [4]. Gao [44] explained that by proposing a
 166 more definitive analytic model called the wavy-crack model, where two velocities are defined: the macroscopic crack

167 velocity v_a and the microscopic local velocity v_c . If the crack speed is above $0.5c_R$, the crack propagates along a wavy
 168 path and the energy absorbed into the crack is used to increase v_c while v_a remains constant. This explains why the
 169 crack speed does not decrease much after branching.

170 Another possible explanation is given by Ravi-Chandar and Knauss [4], who suggested that there exist many
 171 microcracks in front of the main crack as shown in Fig. 3, and branching is a natural outcome of the growth and coa-
 172 lescence of the microcracks. In Homalite-100, a varying fracture surface roughness during branching, ‘mirror’, ‘mist’,
 173 and ‘hackle’, can be observed [14], see Fig. 4. The fracture processes that occur over a spatial domain comparable to
 174 the surface roughness dominate the dynamics of crack growth. Initially, a crack propagates with a mirror-like fracture
 175 surface. Then, because of the coalescence of microvoids or preexisting defects ahead of the crack, the crack surface
 176 may become rough and subsequently microcracks form. The microcracks within the fracture process zone interact
 177 with each other and form micro-branches, which results in the final crack branching.

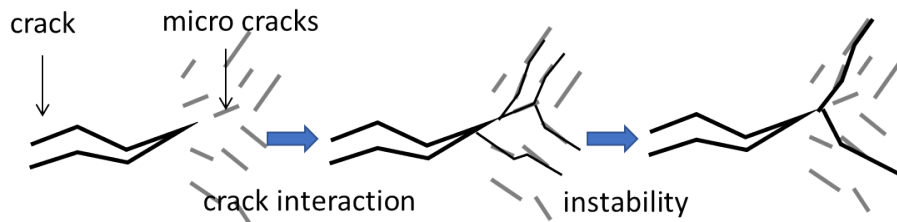


Figure 3: Ravi-Chandar's micro crack model [4].

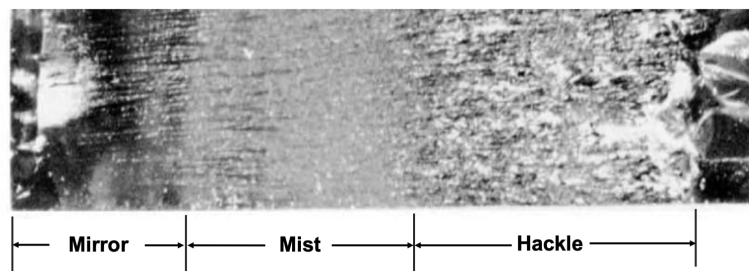


Figure 4: Typical ‘mirror’, ‘mist’ and ‘hackle’ regions are identified in Homalite-100 [14].

178 Following the work of [13, 14, 4, 15], micro-branches and their instability have been studied in great detail
 179 recently by Fineberg et al. [17], Sharon et al. [18], Sharon and Fineberg [19], Sharon et al. [20], Fineberg and Marder
 180 [21], Bouchbinder et al. [22, 23, 24], Livne et al. [25], Fineberg and Bouchbinder [26], Livne et al. [45]. Using
 181 dynamic instabilities, these studies explain a number of long-standing problems in the dynamic fracture of amorphous
 182 including (1) velocity oscillations and limiting velocity, (2) fracture roughness, (3) the origin of the large increase in
 183 the energy dissipation of a crack with its velocity and (4) transition to crack branching. A detailed discussion about
 184 velocity oscillations and limiting is given in § 3.2.1. When the crack velocity exceeds the critical value (limiting
 185 velocity), the velocity begins to oscillate rapidly [17]. A good correlation is demonstrated between the measured
 186 crack velocity and appearance of fracture roughness on the fracture surface [19], see Fig. 5. The initial crack with
 187 a velocity lower than the critical crack velocity v_c corresponds to a mirror-like fracture surface. After achieving the
 188 critical crack velocity v_c , the velocity begins to oscillate. As the velocity increases, rib-like patterns observed on the
 189 fracture surface become more apparent. Microscopic branches have also been observed when the velocity exceeds the
 190 critical value. These characteristic features are independent of the brittle material due to the fact that in two extremely
 191 different classes of material (poly-acrylamide gel and soda-lime glass), identical characteristic behaviour is observed
 192 [45]. The origin of the large increase in the energy dissipation of a crack with its velocity can also be explained by the
 193 micro-branching instability [20]. When micro-branching instabilities occur, the energy dissipation of a crack increases

194 because more surfaces are formed by the micro-branches. As the velocity of the crack increases, transition to crack
 195 branching occurs with the branches becoming longer and more numerous. Micro-branches can smoothly transform
 196 to macro-branches with similar characteristic features of crack branching exhibited between the micro-branches and
 197 macro-branches [18]. The onset of the micro-branching instability therefore provides a well-defined criterion for the
 198 process that eventually culminates in macroscopic crack branching. As the crack velocity increases larger than the
 199 critical velocity, the branch width increases and the surface roughness diverges. This transition may be a sufficient
 200 condition for macroscopic crack branching to occur [19]. The dynamic instabilities have been further studied with a
 201 series of theoretical work [22, 23, 24] and with experiments in brittle gels [25]. A weakly nonlinear theory of dynamic
 202 fracture has been introduced, which implies that the understanding of crack instabilities requires the introduction of
 203 new physical ingredients, e.g. length scales [24]. Intrinsic nonlinear scales in the near-tip region play a decisive role in
 204 dynamic crack instabilities. Fineberg and Bouchbinder [26] gave a comprehensive review of important experimental
 205 and theoretical work in dynamic crack instabilities, which states that the micro-branching instability is an intrinsically
 206 3D instability and to understand the dynamic instabilities, the framework of fracture mechanics should be extended to
 207 include 3D crack propagation.

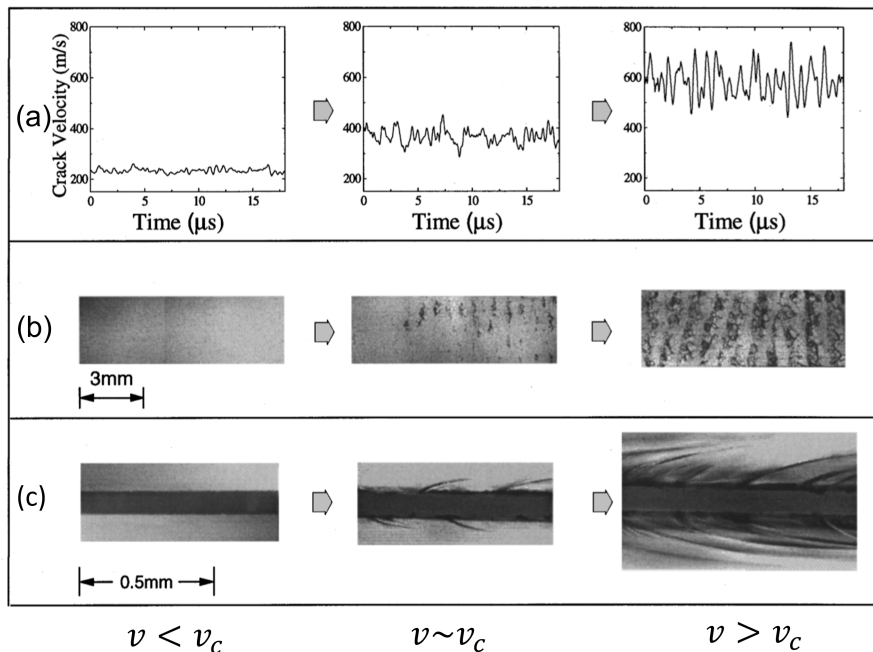


Figure 5: Three aspects of the evolution of the branching instability as the crack propagates from left to right [19]. (a) The velocity of the crack is a smooth function of time when $v < v_c$, the crack velocity starts to oscillate when $v \sim v_c$, the oscillation amplitudes increase when $v > v_c$. (b) The fracture surface is smooth when $v < v_c$, small regions of different texture are distributed along the surface when $v \sim v_c$, these regions coalesce, forming a periodic pattern with wavelength on the order of 1 mm when $v > v_c$. (c) A single crack is observed when $v < v_c$, micro-branches appear when $v \sim v_c$, and increase in length when $v > v_c$.

208 Through theoretical analyses, Adda-Bedia and Arias [46], Adda-Bedia [47, 48], Katzav et al. [49], Adda-Bedia
 209 et al. [50] systematically studied the crack branching mechanisms including dynamic crack instability and 3D micro-
 210 branching instability. Based on the theory of linear elastic fracture mechanics and Eshelby [43]’s energy approach
 211 which states that the energy input into a crack and the energy required to create new branch surfaces must be bal-
 212 anced, the theoretical model for branching instabilities was established [46]. Dynamic crack branching instability
 213 under general antiplane loading [47] and under general loading [48] are studied and the path and geometry of the
 214 branched crack are predicted. It is shown that after branching the in-plane elastic fields immediately exhibit self-
 215 similar properties, and the jump in the energy release rate is maximized. Under this assumption, the crack branching
 216 phenomenon, which is found to be energetically possible, may be seen as a dynamic instability in which a self-similar

single crack propagation would lose its stability at some point dependent on crack velocity [49]. Later, Adda-Bedia et al. [50] investigated the 3D out-of-plane nature of crack front waves (generated by both the interaction of a crack with a localized material inhomogeneity and the intrinsic formation of micro-branches [51]) and the microbranching instability with the Willis-Movchan 3D linear perturbation formalism. It is demonstrated that within a minimal linear elastic fracture mechanics scenario, the existence of an out-of-plane crack front instability is dependent on critical velocity, which may trigger a 3D microbranching instability and its fractographic implications.

For materials like inorganic glasses, where microcracks cannot be found in front of the main crack, different mechanisms have been proposed. Hull [39] suggested micro-scale variations lead to twisting and tilting of the stress vector near the crack tip, cause local instability to the dynamic properties of cracks, and are responsible for the increase of crack surface roughness and crack branching. Sharon et al. [51], Bonamy and Ravi-Chandar [52] tried to explain the surface roughening from the interaction of the shear wave with the tip of the growing crack. The shear wave proves the existence of front waves in dynamic fractures. The front waves feature an out-of-plane component, which leaves marks on the fracture surfaces and causes surface roughness and crack shape perturbations [26].

Though crack branching in dynamic fractures has long been observed and investigated in various literatures, up to now, there has not been a universally agreed-on explanation for crack branching mechanisms. Based on the above work, the mechanisms of branching can be summarized as: (1) the increase of the velocity may cause unstable crack propagation, which causes crack branching; (2) the microvoids and microcracks may increase surface roughness and the growth and coalescence of microcracks which form micro-branches resulting in macro-branches with the energy absorbed in the crack relating to the limiting velocity; (3) the dynamic instability plays an important role. Cracks undergo an oscillatory instability controlled by small-scale, near crack-tip, elastic nonlinearity, and this oscillatory instability may trigger microbranching instability, which provides a well-defined criterion for the process that eventually culminates in macroscopic crack branching; (4) the crack front waves and the tilting and twisting of the stress vector at the crack front may cause local dynamic instability, increasing of crack surface roughness leading to crack branching.

3.2. Branching Criteria

Crack branching criteria tend to be artificially formulated based on physical mechanisms to improve crack branching simulation. We divide the criteria into two types: external criteria and internal criteria. Here, “external” means that in the numerical simulation additional criteria are needed to determine how the crack branching occurs. The criteria required in a whole process for branching simulation include criteria for crack initiation, criteria for crack propagation, criteria for crack branching time and criteria for branching angles. A series of studies on criteria for dynamic crack initiation and crack propagation are summarized in dynamic fracture mechanics [7, 8]. The following discussion will focus on criteria for branching time and branching angles, instead of being exhaustive. In contrast to the “external”, “internal” means that no additional criteria are required, and any occurrence of branching is a natural outcome of the simulation.

3.2.1. External criteria

To determine the branching time, three commonly used criteria are introduced, namely the velocity criterion, the stress intensity factor criterion, and the energy criterion.

Velocity criterion. The velocity criterion suggests that once the crack velocity exceeds a critical value, branching occurs. Note that there exists two branch types, namely micro-branches and macro-branches, which are discussed separately here. Both theoretical and experimental approaches have been used to investigate the critical velocity of a fast moving crack.

An energy balance equation was given by Freund [7], which considers a crack growing with a nonuniform speed under time-independent/dependent loading:

$$G^{dyn} \approx \left(1 - \frac{v}{c_R}\right) K_I^0(t, l(t), 0) = \gamma \quad (1)$$

where G^{dyn} is the dynamic energy release rate, v the crack velocity, $K_I^0(t, l(t), 0)$ the instantaneous stress intensity factor at time t for a stationary crack of length $l(t)$ and γ the fracture energy. Based on Eq. (1), the fracture energy for

262 a moving crack will vanish when the crack velocity v increases to the Rayleigh wave speed c_R . Therefore, from the
 263 elastodynamic fracture mechanics theory, the limiting velocity for crack propagation is no larger than the Rayleigh
 264 wave speed. However, from an experimental view, it is found that only cracks on the cleavage planes in crystalline
 265 materials grow at a rate close to Rayleigh wave velocity. For cracks in noncrystalline materials, the limiting velocity
 266 of the crack is significantly smaller than the theoretically predicted limiting crack velocity [8]. The reason behind this
 267 phenomenon can be explained by dynamic instabilities [17]. Indirect evidence to support this is that when the dynamic
 268 instability is suppressed, the crack may propagate at a supersonic speed [6]. Mechanisms behind the supersonic crack
 269 propagation problems are explored by Buehler et al. [53], Abraham and Gao [54].

270 The critical velocity for micro-branches states that once the velocity exceeds the critical velocity v_c , crack propa-
 271 gation becomes unstable with the occurrence of velocity oscillations, and the increase of surface roughening and
 272 microbranching [21]. The critical velocity for instability and micro-branches has been investigated with experimental
 273 approaches. Fineberg et al. [16, 17] made detailed measurements indicating that the critical velocity for crack propa-
 274 gation in PMMA is $0.36c_R$. Hauch and Marder [28] and Ravi-Chandar and Knauss [14] observed the critical velocity
 275 for crack propagation in Homalite is $0.37c_R$. Gross et al. [55] showed the critical velocity for crack propagation is
 276 $0.42c_R$ in soda-lime glass. Based on the experimental observations above, the existence of a critical velocity for the
 277 instability of brittle fracture may be a universal aspect [17]. Though the micro-branches instability is seen as one of
 278 the reasons for crack branching, the transition from critical velocity criterion for micro-branches to critical velocity
 279 criterion for macro-branches is still unknown [21]. The critical velocity for macro-branches is used to determine when
 280 macro-branches develop. Theoretically, as discussed in § 3.1, various authors established models to analyse the criti-
 281 cal velocity. The critical velocity is assumed to be $0.6c_S$ in Yoffe [41]’s model, $0.5c_R$ in Eshelby [43] and Gao [44]’s
 282 model, $0.52c_R$ in Adda-Bedia [48]’s model. Experimentally, as discussed in § 2, the limiting velocity is $0.5 \sim 0.65c_R$
 283 for glass, $0.6 \sim 0.7c_R$ for PMMA and $0.35 \sim 0.45c_R$ for Homalite-100.

284 In addition, many experimental results show that the crack velocity does not change significantly after branching
 285 [4]. These limitations have challenged or weakened the velocity criterion for crack branching. However, due to its
 286 simplicity, the velocity criterion is widely used in numerical simulation for crack branching. For example, Linder and
 287 Armero [56] proposed a branching model using FEM, where branched elements are added to represent discontinuities
 288 if the crack velocity exceeds a given threshold. The influence of different critical velocities on branching was inves-
 289 tigated with the FEM-based model. Using a similar model, Armero and Linder [57] successfully captured the crack
 290 propagation path and branching characteristics. Xu et al. [58] set up the additional enrichment in XFEM to describe
 291 crack branching and adopted the branching time criterion from Yoffe [41], where the crack branching occurs when
 292 the maximum normalized circumferential stress occurs in two symmetrical directions. The critical velocity during
 293 simulation is found to be over $0.74c_R$. By comparing the numerical result $0.74c_R$ with the experimental result $0.4c_R$,
 294 they concluded that the crack velocity error was due to the velocity criterion adopted.

295 *Stress intensity factor (SIF)*. In elastodynamic fracture mechanics, the theoretical framework is fairly well established
 296 through a series of studies of a dynamically propagating crack in an infinite body by Freund [59, 60, 61, 7]. Taking
 297 mode I crack as an example, the dynamic crack growth criterion is given as:

$$K_I^{dyn}(t, v) = K_{ID} \quad (2)$$

298 where K_I^{dyn} is the dynamic SIF, t the time, and K_{ID} the dynamic crack growth toughness. For the left-hand side of the
 299 Eq. (2), theoretically, the dynamic SIF is related to both the crack velocity and the instantaneous SIF of a stationary
 300 crack, which can be expressed as:

$$K_I^{dyn}(t, v) = k(v)K_I^0(t, l) \quad (3)$$

301 where $k(v)$ is a function of crack velocity and K_I^0 is the instantaneous SIF of a stationary crack with length l at time
 302 t . Numerically, the dynamic SIF can be calculated through J -integral or interaction integral. Unlike the calculation in
 303 quasi-static conditions, the numerical calculation of J -integral or interaction integral is no longer path independent in
 304 dynamics. The reader is referred to the book by Anderson [5] for more details. For the right-hand side of Eq. (2), the
 305 crack growth toughness K_{ID} can be determined experimentally, and the K - v relationship is often employed. Experi-
 306 mentally, the dynamic SIF is related to crack velocity, however, the relationship is not unique, but an average can be
 307 obtained [12, 8], see Fig. 6.

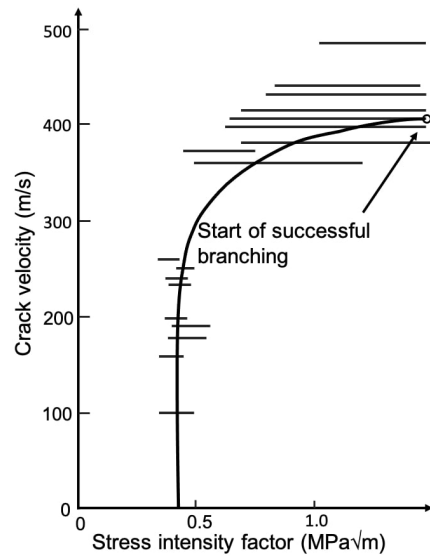


Figure 6: Relationship between crack velocity and stress intensity factor in (brittle) Homalite 100 (solid curve). The “horizontal” lines represent measurements of the tip motion of cracks in large plates as they grow with no or minimal influence of stress waves reflected from the plate boundaries, adopted from [12].

308 By experimental investigations, Kobayashi and Mall [11] and Dally [12] indicated that branching occurs when
 309 the SIF reaches a critical value that is between two and three times the quasi-static fracture toughness of the material.
 310 Clark and Irwin [62] suggested that the dynamic SIF should reach a critical value for branching to occur at terminal
 311 velocity. Based on previous theoretical and experimental studies on crack curving and crack branching, Ramulu and
 312 Kobayashi [3] proposed the following necessary and sufficient conditions for crack branching:

$$\begin{aligned} K_I &\geq K_{Ib} \rightarrow \text{necessary condition} \\ r_0 &\leq r_c \rightarrow \text{sufficient condition} \end{aligned} \quad (4)$$

313 where K_{Ib} is the critical branching SIF, and r_c is the characteristic distance from the crack tip. With experimental
 314 observations, Ravi-Chandar [8] concluded that a crack will split into two or more branches if it reaches the critical
 315 stage identified by its SIF, and each branch will propagate with the same speed as the parent crack. The SIF criterion is
 316 applied to decide crack branching time when modelling crack propagation [63, 64]. Kishen and Singh [63] simulated
 317 crack development (crack kinking and branching) on the rock-concrete interface of a gravity dam using the SIF-based
 318 fracture criterion. Using a time-domain BEM approach, Rafiee et al. [64] examined dynamic crack propagation, where
 319 a critical mode I SIF was used for the branching event and the maximum circumferential stress criterion was employed
 320 for determining the branching angle and each branch’s growth rate.

321 *Energy criterion.* The energy criterion is applicable to both linear and nonlinear fracture mechanics, e.g. the energy
 322 release rate G and the J -integral. The crack extension occurs when the energy available for crack growth is sufficient
 323 to overcome the resistance of the material [65].

324 Eshelby [43] proposed the branching criterion theory based on the balance between the energy inputting into the
 325 crack and the energy required to create new branch surfaces. Based on this study, with the help of the Griffith’s energy
 326 criterion and the principle of local symmetry, Adda-Bedia [47, 48] presented a series of analytical solutions for crack
 327 branching problems. The energy criterion was assumed to be a necessary condition for a branching configuration, and
 328 the stress field in front of the crack tip, the branched shape and the dynamic branching instability were predicted and
 329 analysed. Tchouikov et al. [66] calculated the energy flux per unit time into the crack tip with a dynamic J -integral.
 330 Once a given critical energy release rate is surpassed, the branch occurs and an implicit prediction for branching path
 331 is adopted. Xie et al. [67] derived an energy-based fracture mode for the mode-I crack branching, where branching

332 toughness was proposed, the branching critical energy release rate was derived and the branching angle was predicted.
333 The criterion shows good agreement with the experimental observations reported in the literature.

334 *Criteria for branching angles.* After the branching time is determined, the next step is to determine how the crack
335 propagates with branching. The branching angle has been studied both experimentally and theoretically. Experimentally,
336 as discussed in § 2, the angle subtended by the new branch (immediately after branching) and the original crack
337 plane typically lies between 10° and 45° . Theoretically, the crack propagation direction can be predicted by the maximum
338 circumferential stress theory, the minimum strain energy density factor theory, the principle of local symmetry
339 and the maximum strain energy release rate theory [3]. A comprehensive review of earlier analytical research work
340 on elastostatic and elastodynamic self-similar crack branching problems in homogeneous, isotropic and elastic brittle
341 solids was given by Dempsey [35]. The number of elastodynamic solutions is quite limited compared with the number
342 of elastostatic solutions. For planar elastodynamic crack propagation, Yoffe [41] attempted to explain the branching
343 of cracks by analysing a problem in which a crack of constant length moving along a straight line with a uniform
344 speed in an infinite two-dimensional medium. It is found that the maximum stress moves out of the plane of crack
345 propagation and acts at an angle of 60° to the main crack propagation direction when the velocity is lower than the
346 critical velocity $0.6c_S$. For elastodynamic crack propagation under antiplane loading, Dempsey et al. [68], Burgers
347 [69, 70] derived analytical solutions for a semi-infinite crack that starts to propagate from rest by kinking or branching
348 under the action of a stress pulse loading.

349 To obtain a more general solution for the dynamical crack kinking or branching problem, a series of studies were
350 conducted by Adda-Bedia and Arias [46], Adda-Bedia [47, 48]. To predict the crack path, the determination of the
351 elastodynamic fields associated with kinked or branched cracks is required. Adda-Bedia and Arias [46] presented a
352 new method to determine the elastodynamic stress field/the dynamic SIF associated with the propagation of anti-plane
353 kinked or branched cracks. The theory was applied to the case of dynamic crack branching under general antiplane
354 loading [47] and later the general antiplane loading condition was extended to arbitrary loading condition [48]. The
355 SIF just after branching was given as a function of the SIF just before branching, the branching angle and the branching
356 velocity [48]:

$$K'_l = \sum_m k_l(v') H_{lm}(\lambda, v, v') K_{0m} \quad (5)$$

357 where K'_l and K_{0m} are the dynamic SIF just after branching and the rest SIF just before branching, respectively, l and m
358 $= 1, 2, 3$, $k_l(v')$ is a universal function of the branching velocity v' , and H_{lm} is a dimensionless function of the branching
359 angle coefficient λ , and of the crack velocity before and after branching. When $v' \rightarrow 0$, it can be expressed as:

$$H_{lm}(\lambda, v, v' \rightarrow 0) = F_{lm}(\lambda) \quad (6)$$

360 Taking Mode I crack as an example, to get the branching angle, the Griffith energy criterion and the principle
361 of local symmetry are employed. The Griffith energy criterion states that the energy release rate G during crack
362 propagation is equal to the dynamic fracture energy γ of the material [71]. For crack branching, the relationship
363 between the energy release rate G , fracture energy γ before branching and the energy release rate G' , fracture energy
364 Γ' after branching can be obtained:

$$G' = G \frac{\gamma(v')}{\gamma(v)} \quad (7)$$

365 According to the principle of local symmetry, which states that the crack always propagates in a direction that
366 the local stress field at the crack tip is of mode I type [72], the following conditions are satisfied immediately after
367 branching:

$$g_1(v) = F_{11}^2(\lambda) \quad (8)$$

$$F_{21}(\lambda) = 0 \quad (9)$$

368 where $g_1(v)$ is a decreasing function of the crack velocity v with $g_1(0) = 1$ and $g_1(c_R) = 0$. By solving the equations
369 above, a critical velocity for branching and a branching angle can be obtained. When the velocity exceeds a critical
370 value of $0.52c_R$, a crack starts to branch at a branching angle $\lambda\pi = 27^\circ$ corresponding to $\lambda = 0.15$. The predicted
371 result agrees well with the available experimental results [17, 21]. Detailed analytical solutions for other loading
372 modes were given by Adda-Bedia [48]. Based on the above work, Katzav et al. [49] further summarized the theory
373

374 of dynamic crack branching in brittle materials. With the theory, a systematic analysis of the branching problem is
375 made, and the critical velocity, the branching angle, the branching velocity, and the subsequent branch path described
376 by a curvature parameter are successfully predicted.

377 3.2.2. *Internal criteria*

378 Internal criteria are combined with numerical methods and embedded in the specific crack models, which leads to
379 crack branching as a natural outcome of the simulation. A simple way to judge whether a model or a method contains
380 internal criteria is to check whether branching angle criteria are required during simulation. If not, cracks are allowed
381 to form freely in the simulation. Models and methods containing internal branching criteria include, but are not limited to,
382 the cracking particles method, the peridynamics, the phase field model, the element deletion model, the cohesive
383 zone model, the enrichment models and nonlocal models/gradient models/viscous models. Among them, the cohesive
384 zone model, the cracking particles method, the phase field model, and the peridynamics, which are representative, are
385 briefly introduced in this section, while more detailed information about all these models and methods can be found
386 in § 4.

387 In the cohesive zone model, the traction-separation law defines the relationship between the crack width (distance
388 between the crack surfaces) and the cohesive traction in the process zone. The crack surfaces begin to separate when
389 the cohesive strength is reached, and when the separation reaches a critical value, the traction decreases to zero and
390 failure occurs. Crack branching naturally forms in the solution of the initial-boundary value problem without any
391 branching criteria [73, 74]. In the cracking particles method, the crack is described by the set of cracked particles
392 [75, 76, 77]. A cracking criterion is employed to crack the particle and create a discrete crack. The crack is modelled
393 by a set of discrete cracks. During simulation, no external criteria are required to determine the branching time and
394 branching angles, and the crack develops by breaking particles in a sequence. In the peridynamics, the material can
395 be considered as a collection of points [78]. If as a result of various forces, two points of the material are separated by
396 a distance beyond a critical value, the interaction (bond) between the two points will vanish (break). Only one critical
397 value for a bond break is needed. Once the stretch exceeds the critical value, failure starts to occur and under certain
398 boundary conditions, crack branching is observed without additional criteria for branching [78]. The phase field model
399 is developed in the form of a variational theory of fractures based on the principle of minimum total potential energy.
400 Through defining the total potential energy of a material body with cracks, it turns the crack propagation problem
401 into an energy minimization problem. By giving boundary conditions, the unknown displacements and the crack path
402 can be solved via global minimization. Thus, in theory, there is no need of external branching criteria, and the only
403 rule required for crack initiation or propagation is that: compared to the previous configuration, the new configuration
404 leads to the lower total energy. Similarly, crack branching is allowed if lower potential energy can be obtained than a
405 simple extension.

406 4. Crack models and numerical methods

407 Crack models are used to describe how to represent the fracture, including the geometry and the stress concen-
408 tration. Numerical methods are employed to solve equations, describe the bulk material behaviour, and capture the
409 fracture propagation process. Different models can be combined with each other and they can be integrated with
410 multiple numerical methods. Likewise, different numerical methods can be combined to form hybrid methods, and
411 they can also work with different fracture models, see Fig. 7. Smear crack models can account for the crack tip nonlin-
412 earity. While discrete fracture models integrated with notable methods such as finite element method, extended finite
413 element method, boundary element method often do not account for crack tip nonlinearity unless the cohesive zone
414 model is employed.

415 4.1. *Crack models*

416 Crack models are used to describe how to represent the crack, and they can be roughly divided into two categories:
417 discrete crack models and smeared crack models. Based on how the crack is represented, the “discrete” means the
418 crack topology is explicitly represented while the “smeared” means the crack is smeared over a certain width without
419 explicit tracking of crack surfaces. Popular discrete crack models include remeshing, element deletion, cracking
420 particles, and enrichment models. Popular smeared crack models include phase field, nonlocal, gradient and viscous

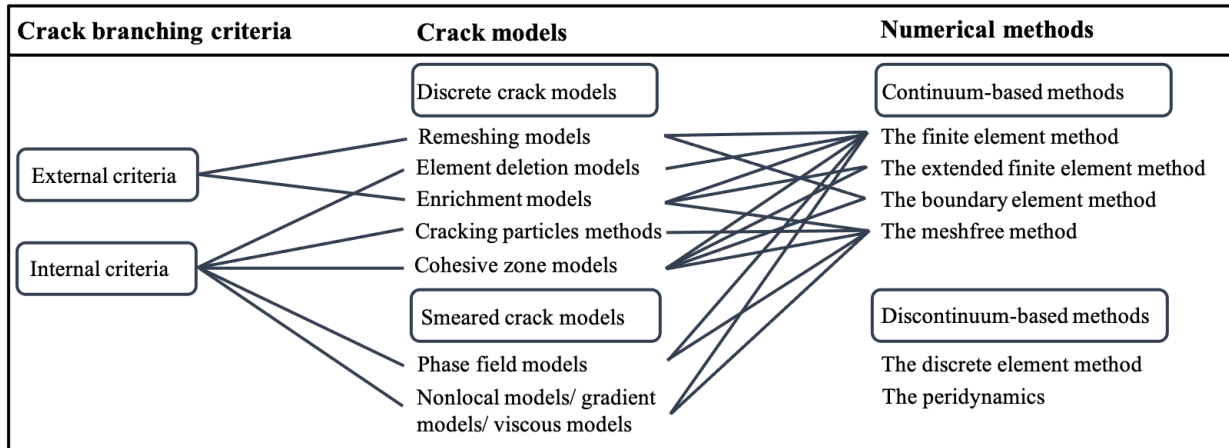


Figure 7: Crack models and numerical methods.

421 models. Note that different from the models mentioned above which describe how to represent cracks, the cohesive
 422 zone model describes the nonlinear behaviour in the process zone ahead of the crack tip with a traction-separation
 423 law and it is essentially a discrete concept. Therefore, we describe the cohesive zone model as part of the discrete
 424 crack models. However, it can also be implemented in smeared context by distributing the work of separation or
 425 fracture energy over the width of an element [79]. See [80] for various smeared representations of cohesive-zone type
 426 behaviour. As a summary, Table. 2 lists the advantages and limitations of different crack models, and their details are
 427 separately discussed in the following subsections.

Table 2: Advantages and limitations of different crack models for crack branching.

Crack Models	Advantages	Limitations
Remeshing models [2, 66]	flexible in dealing with complex geometries and boundary conditions	awkward in dealing with complex three-dimensional geometries
Element deletion models [81, 82, 83]	easy implementation	special treatment is required to solve the mesh dependency
Enrichment models [84, 85, 86]	solve parts of difficulties associated with the mesh	rely on different types of enrichment adopted, see more detail in § 4.2
Cracking particles methods [75, 76, 77]	suitable for complex crack patterns, straightforward implementation in 3D	special treatment is required to solve the “spurious cracking” problems and reduce the computational cost
Cohesive zone models [73, 74]	suitable for complex crack patterns, removes singularity in the crack tip	special treatment is required to solve the mesh dependency and bias
Phase field models [87, 88]	suitable for complex crack patterns, straightforward implementation in 3D	fine mesh is required to obtain more accurate results
Nonlocal models/gradient models/viscous models [89, 90]	solve the ill-posed boundary value problem, suitable for modelling failure caused by progressive damage	physical inconsistencies may appear, fine mesh is required to obtain more accurate results

428 4.1.1. Discrete crack models

429 *Remeshing models.* As the crack propagates and branches, new discontinuities form across the crack, therefore, crack
 430 surfaces need to be redefined as boundaries and the mesh needs to be updated. Remeshing models update the crack
 431 surface with remeshing techniques, where an explicit representation of crack surfaces and a crack tracking algorithm
 432 are usually required. During the simulation process, external criteria including the crack initiation, propagation,
 433 branching time and angle criterion are employed, which increases the difficulty of computational simulation. The
 434 reasons are manifold: (1) until now, there is no universally agreed explanation for branching time and branching

435 angles; (2) the formula to calculate the associated parameters under dynamic situation remains a challenge; (3) a
 436 remeshing rule including the selection of element type, mesh generation method, data transfer during remeshing is
 437 required for which computation efficiency needs to be considered.

438 The remeshing models can be combined with such numerical methods as FEM and BEM to simulate crack branching.
 439 A schematic illustration of crack branching with remeshing models based on FEM is shown in Fig. 8. Compared
 440 with remeshing models based on FEM, remeshing models based on BEM is much simpler due to the reduced dimen-
 441 sional features of BEM. Details will be explained in § 4.2. Both methods assume that the crack surface is generally
 442 determined by the separation between elements, which makes it difficult to capture crack surface roughness relating
 443 to dynamic brittle fracture. Note that another commonly used application of the remeshing models is its combination
 444 with cohesive zone models by actively inserting cohesive interface elements into the finite element mesh, which will
 445 be discussed separately later.

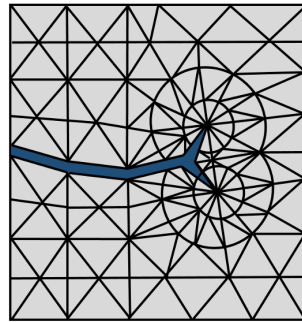


Figure 8: A schematic illustration of crack branching with remeshing models based on FEM.

446 *Element deletion models.* Element deletion models are often integrated with FEM, where the crack is represented by
 447 a set of deleted/deactivated elements, as shown in Fig. 9. There is no need for explicit representation of the crack’s
 448 topology by remeshing. The deactivation of elements can be achieved through two approaches: (1) complete element
 449 deletion technique, in which deleted elements are replaced by rigid masses and (2) setting the stress of the deactivated
 450 elements to zero [81, 91]. The elements, which are deactivated or deleted, have no material resistance or stress for the
 451 rest of the simulation process [92].

452 However, unless the constitutive equation is properly scaled or adjusted, the released energy due to deleting an
 453 element will depend on the element size, which can cause spurious mesh dependency and lead to high computational
 454 cost in dynamic crack simulations [93]. To reduce the spurious mesh dependency, the softening curve slope should be
 455 scaled so that fracture energy is independent of the element size [81]. The mesh dependency problem is also handled
 456 with variational formulations [82]. Schmidt et al. [94] proposed a promising approximation scheme named “eigen-
 457 fracture”, in which the deformation is seen as an eigen-deformation in the eroded element and a nonlocal regularized
 458 fracture energy is introduced to eliminate the mesh dependence. Derived from the eigenfracture, Pandolfi and Ortiz
 459 [82] developed a method called “eigenerosion”, which is characterized by the restriction of element erosion in a binary
 460 sense: it can be equal to 0 if the element is eroded or 1 in case of fully elastic behaviour. The fracture propagation
 461 is then treated as failing elements when the elastic energy release is higher than the corresponding dissipated frac-
 462 ture energy. Compared with the original element deletion model, the eigenerosion, as an extension version, is more
 463 suitable for crack branching problems for its accuracy and convergence in complex crack simulations [81, 82, 83, 94].

464 Song et al. [81] checked the performance of the element deletion model for dynamic crack propagation in brittle
 465 materials and found that the element deletion model gives a very irregular crack velocity and performs poorly for the
 466 accurate prediction of crack branching. Based on the eigenerosion, Stochino et al. [83] introduced a modified formu-
 467 lation of eigenfracture, where the compression and tension loaded state is distinguished. The efficacy of the approach
 468 is proved by a dynamic crack branching example. It is found that the crack branching time depends on the frac-
 469 ture resistance of the structure related to the critical energy release rate and numerical parameter settings. To reduce
 470 the high computational cost caused by a relatively fine mesh during modelling, Fan et al. [95] presented a dynamic
 471 adaptive eigenfracture scheme by combining the eigenfracture scheme and the adaptive mesh refinement algorithm,

472 which reduces the element size locally while improving the Griffith fracture convergence property. The ability of the
 473 dynamic adaptive eigenfracture scheme in predicting crack propagation was proved by numerical examples of crack
 474 branching, see Fig. 10. It is found that the crack pattern, the crack branching velocity and crack instabilities in the
 475 simulation are in good agreement with the experimental observations.

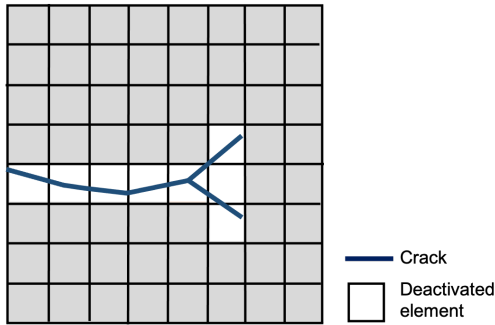


Figure 9: A schematic illustration of crack branching with element deletion models.

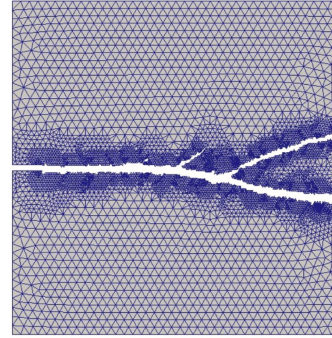


Figure 10: A numerical example of crack branching with element deletion models [95].

476 The element deletion model deletes elements that satisfy a certain criterion explicitly and no additional criteria are
 477 required to determine the branching time and branching angles. However, special treatment is required to solve the
 478 mesh dependency problem [93]. The mesh needs to be fine enough to obtain accurate crack path prediction in dynamic
 479 crack simulations, which may in turn cause high computational cost. To the best of the author’s knowledge, till now,
 480 the number of studies on the performance of the element deletion model in dynamic crack branching simulation is
 481 limited [81, 83, 95], and no 3D examples are provided. Though its ability in modelling the crack pattern and the crack
 482 branching velocity has been proved in 2D [95], more investigations such as multiple crack branches, crack branching
 483 in 3D are yet to be demonstrated.

484 *Enrichment models.* The enrichment models use the so-called “enrichment approaches” to account for the discon-
 485 tinuous displacement fields in the crack. The enrichment approach is to enrich a polynomial approximation space so
 486 that the crack can be modelled independently of the mesh. There are commonly two types of enrichment, namely,
 487 the intrinsic enrichment and the extrinsic enrichment. The intrinsic enrichment is to replace (at least some of) the
 488 shape functions in the polynomial approximation space with special shape functions. The number of shape functions
 489 and unknowns is unchanged during simulation. While the extrinsic enrichment can be achieved by adding special
 490 shape functions to the polynomial approximation space, where more shape functions and unknowns result in the
 491 approximation [96].

492 The enrichment model can be combined with XFEM or MMs. Fries and Belytschko [96] summarized important
 493 features about enrichment in XFEM: (1) the enrichment is extrinsic and realized by the partition of unity (PU) concept;
 494 (2) the enrichment is local because only a subset of the nodes is enriched; (3) the enrichment is mesh-based, i.e. the
 495 PU is constructed using standard FE shape functions; (4) enrichments for arbitrary discontinuities in the function
 496 and their gradients are available. A schematic illustration of crack branching with enrichment models combined with
 497 XFEM is shown in Fig. 11. Compared with the enrichment in XFEM, the enrichment in MMs can be both intrinsic and
 498 extrinsic. The extrinsic enrichment can be further classified into an extrinsic moving least-square (MLS) enrichment
 499 and an extrinsic PU enrichment. The ability of the model in capturing crack branching differs with the methods it
 500 combines, detailed explanations will be given in § 4.2.

501 *Cracking particles methods.* In the cracking particles method (CPM), the crack is modelled by a set of discrete cracks.
 502 As shown in Fig. 12, the discrete crack is restricted to lie on the particles. Since the crack is described by the set of
 503 cracked particles, no representation of the crack’s topology is needed [75, 76, 77]. The method was first developed
 504 by Rabczuk and Belytschko [75]. In the model implemented with the cracking particles method, the displacement
 505 approximation is given by:

$$\mathbf{u}^h(\mathbf{x}) = \sum_{i \in N} \hat{N}_i(\mathbf{x}) \mathbf{u}_i + \sum_{i \in N_c} N_i(\mathbf{x}) S(f_i(\mathbf{x})) \mathbf{q}_i \quad (10)$$

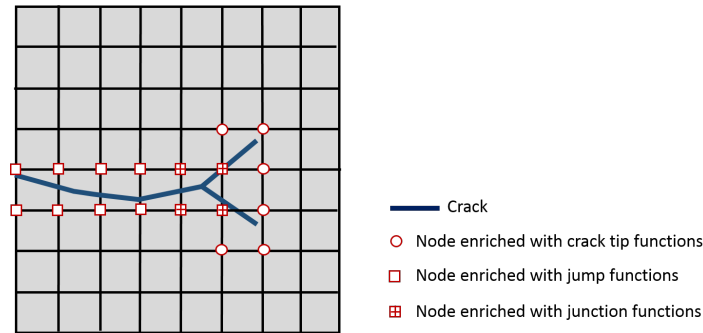


Figure 11: A schematic illustration of crack branching with enrichment models combined with XFEM.

506 where \mathbf{u}_i is the displacement vector, N and N_c are the total set of nodes in the model and the set of cracked nodes
 507 respectively; \hat{N}_i and N_i are the continuous and discontinuous shape functions, respectively; $S(f_i(\mathbf{x}))$ is the sign function
 508 defined as 1 and -1 on two sides of the crack parametrized by \mathbf{q}_i . Therefore, the displacement jump across the crack
 509 can be obtained from Eq. (10):

$$[[\mathbf{u}]] = 2 \sum_{i \in N_c} N_i(\mathbf{x}) S(f_i(\mathbf{x})) \mathbf{q}_i \quad (11)$$

510 A discrete crack is introduced whenever a cracking criterion is met at a particle [75]. The cracking criteria
 511 differ with different material properties, e.g. loss of hyperbolicity is used for a rate independent material while loss
 512 of material stability is used for a rate dependent material [97]. The reader is referred to [86] for a more detailed
 513 description of commonly used cracking criteria.

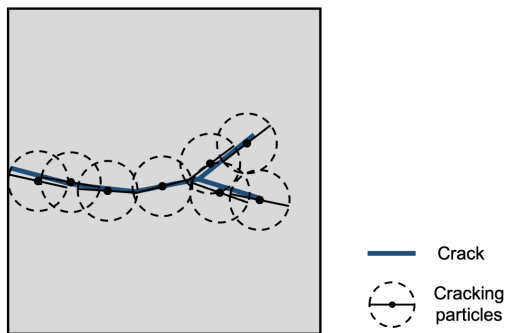


Figure 12: A schematic illustration of crack branching with CPMs.

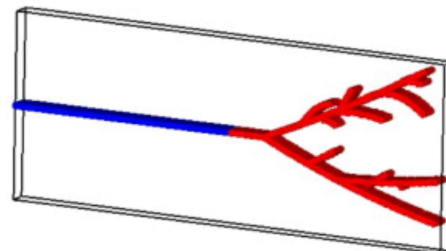


Figure 13: A 3D example of crack branching with CPMs [76].

514 Based on the original model, Rabczuk and Belytschko [76] extended its application to three dimensional problems,
 515 where a continuous crack is represented by a contiguous set of cracked particles. The sphere particles are separated
 516 by a crack plane that passes through the centre of the particle. The method proves its capability in large deformations
 517 and arbitrary nonlinear and rate-dependent materials with different examples. A crack branching example in 3D with
 518 CPM is given, see Fig. 13. The crack front line is almost linear without capturing the fracture tunnelling feature. The
 519 reason may be the use of brittle materials while fracture tunnelling is often observed in ductile materials. Since the
 520 crack pattern along the out-of-plane direction is uniform, this example can be considered as a “2.5D” example. To
 521 further prove the ability of the method to simulate a real 3D problem, a non-planar crack growth example is given
 522 in [76], which is not shown here since this non-planar crack growth example does not include the crack branching
 523 phenomenon. Later, Rabczuk et al. [77] further developed the model avoiding the requirement of the enrichment.
 524 By splitting particles where the cracking criteria are met into two particles on opposite sides of the associated crack
 525 segments, the crack is modelled with no additional degrees of freedom being added in the formulation. By various
 526 benchmark examples, the model proves its capability in modelling complex crack patterns in statics and dynamics.
 527 Using the CPM, Rabczuk et al. [98] studied the instability in dynamic fracture and reproduced the experimentally

528 observed results, including the limiting velocity, microcrack branching and increase of energy dissipation. It is found
 529 that the existence of voids in the model has little effect on the occurrence of microcrack branching. To solve the
 530 spurious cracking problems which appear in the original CPM [75], Ai and Augarde [99] improved the crack path
 531 curvature modelling through bilinear segments with consideration of cracking angle changes at particles, which allows
 532 crack kinks inside a particle. The model was further improved by the so-called “multi-cracked particle method” [100],
 533 which can deal with branched cracks (tree-shaped cracks) by splitting a cracking particle multiply. However, all the
 534 numerical examples in Ai and Augarde [100]’s work are limited in linear elastic fracture mechanics problems and
 535 no dynamic crack branching example is provided. Though solving the spurious cracking problem, the methodology
 536 only proves its ability in modelling branched crack (tree-shaped cracks), not the dynamic crack branching process.
 537 This is due to the cracking rule it adopted prevents crack branching. The spurious cracking problem was also solved
 538 by Xu [101], where a stable CPM based on nodal integration and updated Lagrangian kernels are proposed and a set
 539 of simple cracking rules are suggested. Crack branching examples are studied and the existence of limiting velocity
 540 observed in dynamic crack branching experiments is proved with the simulation results.

541 In summary, the CPM is quite suitable for problems with complex crack patterns, especially crack branching.
 542 The CPM has the following advantages: (1) no representation of the crack’s topology and no crack path continuity
 543 are needed; (2) crack branching can happen automatically, no additional branching criteria are needed, and dynamic
 544 instabilities related to micro-branches can be captured; (3) it is easily implementable in 3D; (4) no mesh orientation
 545 problem. On the limitation side, it is noted that: (1) due to the “discontinuous” representation of the crack surface,
 546 special techniques are required to solve the “spurious cracking” problems; (2) since the crack path is approximated
 547 via a collection of cracking particles, a finer node distribution is required to increase the accuracy of the model, which
 548 may increase the computational cost.

549 *Cohesive zone models.* The cohesive zone model (CZM) is developed to describe the nonlinear behaviour during
 550 material failure. It assumes a process zone ahead of the real fracture [102, 103], where a traction-separation law
 551 controls the variation of cohesive traction with the separation (width) of the crack. When the maximum principal
 552 stress reaches the cohesive strength of the material T_{max} , the crack initiates. With the crack opening, the cohesive
 553 traction will decrease and once it has decreased to zero, the maximum crack opening w_{max} is obtained and complete
 554 separation is reached. There are many types of traction-separation laws, such as the exponential form [103], the
 555 polynomial form [104], the bi-linear form [105] and the linear form [106]. Park and Paulino [107] gave a critical
 556 review on these laws and their physical and numerical properties. Depending on the characteristics of the traction-
 557 separation law, the CZMs can be divided into two groups: the intrinsic and extrinsic CZMs. As shown in Fig. 14.
 558 In the intrinsic CZM, the cohesive traction first increases with the crack opening at an initial stiffness K_c , while the
 559 extrinsic CZM does not have the initial stiffness.

560 Since the CZM is generally a concept to describe the nonlinear behaviour in the process zone, it can be incorpo-
 561 rated with different numerical methods and crack models [79]. For example, it can be employed in XFEM and phase
 562 field model by introducing a length scale. For discrete cracks in a finite element context, cohesive interface elements
 563 (elements equipped with a traction-separation law) have been employed extensively. The simulation process of crack
 564 branching modelling with CZMs using cohesive interface elements is further discussed in the following paragraphs.

565 To model crack branching with the intrinsic CZM, the deformation equation first needs to be given and the domain
 566 needs to be divided into elements. Then, cohesive interface elements need to be assigned on all finite element surfaces
 567 before simulation. Finally, the displacement field is solved with the traction-separation law. During this process,
 568 remeshing is not required and the crack is allowed to propagate along element boundaries. No external criterion is
 569 needed for crack branching since the branching phenomenon emerges as a natural outcome of the initial-boundary
 570 value problem solution [73]. However, because the finite initial slope of the traction-separation law modifies the
 571 stiffness of the structure and alters the wave propagation, the intrinsic CZM has issues such as the artificial softening
 572 effect, loss of consistency, spuriously high crack velocity (the lift-off issue) (see [108] for a complete discussion about
 573 these issues). A remedy to reduce the effect of artificial compliance is to increase, if possible, the initial elastic slope
 574 of the traction-separation law, which results in severe stable time step restrictions and may even render the intrinsic
 575 approach unsuitable for explicit dynamic calculations, or in ill-conditioning of the tangent stiffness matrices in static
 576 or implicit dynamics analyses.

577 The process for modelling crack branching with the extrinsic CZM is similar to the intrinsic CZM. The difference
 578 lies in the cohesive interface elements, which is illustrated in Fig. 15. Instead of inserting all cohesive interface ele-

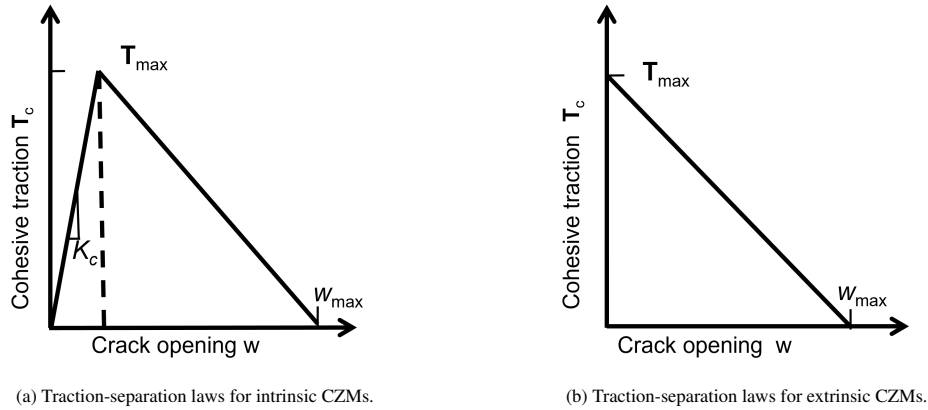


Figure 14: Traction-separation laws for CZMs.

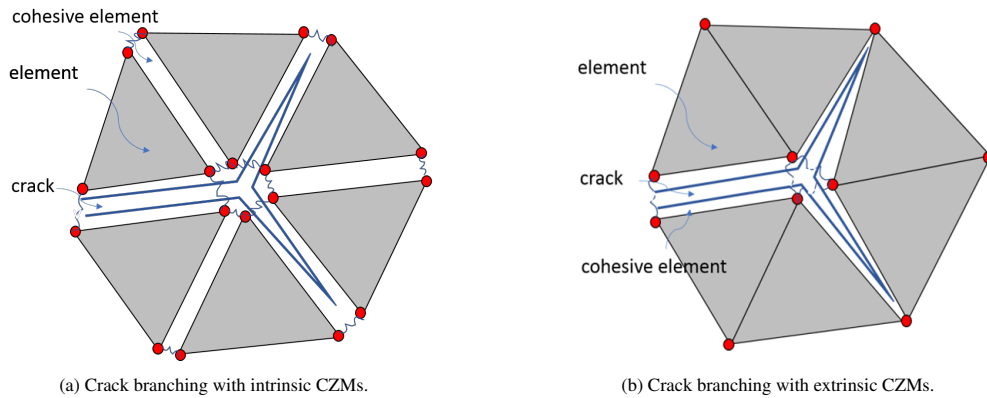


Figure 15: Crack branching with CZMs.

579 ments first, cohesive interface elements will be assigned adaptively when the criterion (the cohesive traction reaches
 580 the cohesive strength T_{max}) is satisfied [74]. By doing so, it avoids the artificial softening effects, however, additional
 581 issues of the efficient parallelization of extrinsic cohesive interface elements with the change in mesh topology need
 582 to be addressed. In addition, the extrinsic CZM has the time discontinuity issue (the traction before and after inser-
 583 tion/activation of an interface element may not be continuous). This is because before cracking, the cohesive traction
 584 depends on the stress field within the neighbouring continuum elements while in the subsequent time step following
 585 cohesive element insertion, the cohesive traction relies on the cohesive law [108]. The time discontinuity leads to
 586 oscillatory behaviour, non-convergence in time and dependence on nonphysical regularization parameters [109]. To
 587 solve this, different approaches have been proposed to make sure the time continuity condition (the continuity of
 588 traction before and after insertion/activation of an interface element) is satisfied [109, 110, 111].

589 Both intrinsic CZMs and extrinsic CZMs have the problem of mesh dependency and bias since the cracks are
 590 only allowed to propagate along element facets. Arias et al. [112] modelled the macroscopic crack branching with
 591 the extrinsic approach and concluded that the occurrence of branching may be very sensitive to the mesh parameters.
 592 Due to the dependence on mesh, the crack paths predicted tend to be somewhat inaccurate. The problem can be
 593 remedied by finer mesh or special mesh operations. Agwai et al. [113] found that finer and unstructured mesh performs
 594 better than coarser and structured mesh in predicting the branching pattern observed experimentally by investigating
 595 the different levels of mesh refinement for both structured and non-structured meshes. Special operations, such as
 596 nodal perturbation and edge-swap topological operation [114], splitting of polygonal finite elements [115, 116], stress
 597 recovery and domain integral [117] are also proposed to reduce and remove mesh bias and dependency in CZMs, by
 598 which physical phenomena associated with dynamic crack branching are successfully captured.

599 Many successful applications can be found in modelling crack branching using CZMs. With the intrinsic CZM,
 600 Xu and Needleman [73] successfully modelled the crack branching phenomenon. The results show that the branch-
 601 ing phenomenon has a close relationship with the applied loading and the dynamic crack velocity computed by the
 602 intrinsic CZM is in good agreement with experimental observations. By using an advanced topological data structure
 603 representation, Zhang et al. [118] presented the extrinsic cohesive modelling of dynamic fracture and emphasised the
 604 importance of adopting the extrinsic CZM for the simulation of multiple micro-branches where the results yield im-
 605 proved agreement with experimental results compared to Miller et al. [119], which employs a potential-based intrinsic
 606 CZM for the same problem. As shown in Fig. 16, complex crack branching patterns including both multiple branches
 607 and micro-branches are predicted. After investigating the micro-branching process, the numerical results reveal that
 608 the increased energy input leads to increased crack surface roughness, longer micro-branches and higher crack speed.
 609 Paulino et al. [114] proposed an extrinsic cohesive zone model using nodal perturbation and edge-swap operators and
 610 proved the capability of the model in providing consistent results between experiments and computational simulation
 611 in terms of microbranching patterns and crack velocity. Park et al. [120] proposed adaptive mesh refinement and
 612 coarsening schemes for efficient computational simulation of dynamic cohesive fracture, which successfully captures
 613 small branches observed experimentally before the crack branching. It is shown that the formation of micro-branches
 614 leads to a lower main crack velocity, which is closer to experimental observations. Though this work uses an advanced
 615 topology-based data structure to store the FE discretization and realize parallelization, examples in three dimensions
 616 are not given due to the complexity of the implementation of the extrinsic approach. For more complex problems
 617 like dynamic fracture propagation in three dimensions, the hybrid discontinuous Galerkin cohesive element method
 618 has been adopted [121]. The cohesive interface elements are assigned first on all element surfaces before simulation
 619 and are not allowed to open by a discontinuous Galerkin formulation. The model is then switched to the extrinsic
 620 cohesive crack model when a failure criterion is met. The method is capable of modelling large-scale dynamic crack
 621 propagation in three dimensions with powerful computers since it saves from the trouble of extensive updating of
 622 mesh information and avoids issues that intrinsic cohesive interface elements bring. Radovitzky et al. [110] presented
 623 a scalable 3D fracture and fragmentation algorithm based on the hybrid discontinuous Galerkin and cohesive ele-
 624 ment method and demonstrated its ability in capturing intricate patterns of cracks including branching. Becker and
 625 Noels [122] presented a full-Discontinuous Galerkin formulation of nonlinear Kirchhoff–Love shells and combined it
 626 with CZMs to perform thin body fracture simulations. Three-dimensional simulations including crack branching are
 627 given, see Fig. 17. Baek et al. [123] proposed a computational framework for multiscale dynamic fracture analysis,
 628 where micro-scales and macro-scales are integrated by introducing an adaptive microstructure representation. A Park-
 629 Paulino-Roesler (PPR) potential-based CZM was presented in [124, 125], which yields a consistent traction-separation
 630 relationship for an arbitrary separation path [126]. The self-interpenetration during dynamic fracture simulation was
 631 avoided by employing a simple penalty method [127] and the nonlinear dynamic fracture behaviour associated with
 632 spontaneous multiple microcrack initiation and branching in conjunction with the microstructure was investigated.
 633 The results show that the microstructure should be carefully considered for dynamic cohesive fracture investigations.



Figure 16: A 2D example of crack branching with CZMs [118].

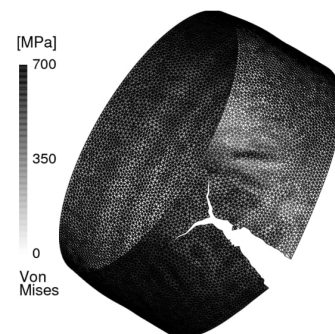


Figure 17: A 3D example of crack branching with CZMs [122].

634 In summary, the CZM is a good choice for the study of dynamic crack branching and can be combined with
 635 different models and methods to describe the nonlinear behaviour of the crack. With cohesive interface elements, it

is easily incorporated into a finite element framework and has the ability of detecting crack initiation and capturing multiple branches and micro-branches. The mesh dependency problem it suffers can be solved by refining meshes or other special mesh operations, which in turn, may increase the computational cost and complexity of implementation procedure, especially in 3D. A promising approach to avoid these problems is the combination of the cohesive law and the discontinuous Galerkin formulation. Explanations about the approach and its application in dynamic fractures including branching can be found in [108, 110, 121, 123, 128, 122].

4.1.2. Smearred crack models

Phase field models. As a recently emerged model, the phase field model (PFM) smears the crack over a certain domain without tracking the crack surfaces. Based on the principle of minimum total potential energy, the PFM solves a fracture problem as an energy minimization problem. The energy functional for simulating crack propagation is first given by Francfort and Marigo [129]:

$$E(\mathbf{u}, \Gamma) = \int_{\Omega} \Psi(\epsilon(\mathbf{u}))d\Omega + G_c \int_{\Gamma} d\Gamma \quad (12)$$

where Ω is a domain describing a cracked solid, Ψ denotes the elastic energy density, $\epsilon(\mathbf{u})$ is the strain field, and G_c is the fracture toughness, which yields an admissible crack set $\Gamma \subset \Omega$. \mathbf{u} is the displacement field and is discontinuous across Γ . Bourdin et al. [87] devised its regularized formulation:

$$E_\varepsilon(\mathbf{u}, \phi) = \int_{\Omega} f(\phi)\Psi(\epsilon(\mathbf{u}))d\Omega + G_c \int_{\Omega} \left(\frac{1}{4l_0}(1 - \phi)^2 + l_0|\nabla\phi|^2 \right) d\Omega \quad (13)$$

where ϕ is damage-like crack phase-field parameter with 1 representing the unbroken part and 0 the totally broken part. $f(\phi)$ is the energetic degradation function to help prevent numerical difficulties where the material is broken (e.g. $\phi = 0$). The width of transition zone is controlled by the length scale l_0 . When l_0 is very small, the diffusive crack presented by the phase field would approximate a sharp crack solved in discrete crack approaches. With the help of Eq. (13), the scalar field (the phase field) turns the intact material into a broken material smoothly instead of treating cracks as strong discontinuities. This enables PFM to overcome difficulties in modelling complex crack problems in three dimensions with traditional numerical methods. Because the propagation of the crack is obtained through the solution of the differential equation, the PFM also avoids the need of additional criteria for crack propagation and additional work to track the fracture surface algorithmically [88, 130].

The ability of PFM to simulate crack propagation and branching in two and three dimensions has been demonstrated [88, 131, 132, 133, 134, 135]. Borden et al. [88] extended the quasi-static phase-field crack model to a dynamic model and used both 2D and 3D crack branching examples to show that the combination of the phase-field model and local refinement strategy is an effective method for simulating complex crack problems. Hofacker and Miehe [131] established a phase field model based on variational principle and demonstrated its performance by means of representative 2D and 3D quasi-static and dynamic model problems including branching. Bleyer and Molinari [132] investigated the microbranching instability occurring in dynamic crack propagation with a 3D variational phase-field model and showed that the microbranching process is a three-dimensional instability and the branching patterns are strongly influenced by phase-field internal length scale. To overcome the limitations of the strong dependence of crack branching patterns on internal length scale, a regularized phase field based cohesive model was introduced by Wu and Nguyen [133], Wu [134], Nguyen and Wu [135], which is insensitive to the length scale and capable of capturing multiple crack branching.

Compared with remeshing models which need the separation between the elements to describe the crack surface, PFMs are capable of modelling multiple branches, widening of damage zone (fracture roughness) and micro-branches. Regarding multiple branches, Zhou et al. [136] Zhou et al. [137] and Ren et al. [138] presented PFMs for simulating complex crack patterns. Multiple crack branches phenomenon is observed, which demonstrates the advantages of PFM in modelling complex crack propagation in rocks. Regarding micro-branches, it refers to the branch of which length is in order of length-scale of simulation [34]. Fig. 19 shows a 3D crack branching example with micro-branches based on PFM. From the figure, a slightly curved crack front (the crack tunnelling feature) and slightly rough crack surfaces can be observed. Regarding the widening of the damage zone before branching, it can be seen as

679 an increase in fracture surface roughness prior to branching, which has been observed in experiments [3]. According
 680 to the branching mechanism proposed by Ravi-Chandar and Knauss [13, 14, 4], a widening damage process-zone
 681 appears before crack branching due to the increasing fracture roughness (mirror-mist-hackles transition). Then, after
 682 branching, as the crack branches go on propagating, the damage zone become “thinner”, indicating that the crack
 683 surfaces turn smooth again. If the energy provided is sufficiently high, the “widening-thinner process” is repeated,
 684 and secondary branches can be observed. Fig. 18 shows a 2D crack branching example, where the widening of the
 685 damage zone before branching and multiple branches can be observed.

686 Given its strong ability in modelling crack branching without remeshing and external criteria, more authors choose
 687 to apply PFM for the study of the dynamic crack branching aiming at providing new analyses of the mechanisms
 688 behind this phenomenon. The crack velocity, the crack branching angle, the crack branching criterion, as well as the
 689 sensitivity of numerical simulation parameters to crack branching are studied.

690 In terms of the crack velocity, since the crack tip is not uniquely defined in PFM [131], a number of approaches
 691 are proposed to measure the crack tip position. Borden et al. [88] proposed to calculate the propagation velocity
 692 explicitly by finding the crack tip with a certain defined phase-field value. Wu et al. [139] computed the crack speed
 693 from using the slope of the line that best fits the three points, in a least square sense. Hofacker and Miehe [140]
 694 tried to obtain the velocity implicitly by using the crack surface velocity to represent the crack speed. All of the
 695 approaches are reasonable due to the definition of the crack tip position being physically implicit in PFM. Regarding
 696 the branching angle, similar conclusions are made by Wu et al. [139], Hofacker and Miehe [140] that with increasing
 697 loading amplitude or velocity, the crack branches earlier and the branching angle gets smaller. Various branching
 698 criteria have been examined. Henry [141] studied crack propagation in two dimensions using the PFM and believed
 699 that the branching instability starts with a critical speed of $0.48c_S$, where c_S is the shear wave speed. Wu et al. [139]
 700 denied the validity of the velocity branching criterion by proving that crack speed at the moment of branching is very
 701 sensitive to the width of the sample with a 2D PFM model. Instead of crack velocity, Hofacker and Miehe [140]
 702 preferred the phase field velocity and the crack surface velocity as local and global indicators for branching. Through
 703 studying the limiting velocity, crack branching and velocity-toughening mechanisms with the PFM, Bleyer et al. [34]
 704 proposed that the branching occurs when the local energy release rate exceeds twice the critical energy release rate. By
 705 quantifying the energy flux into the crack tip and fracture energy, Tian et al. [142] confirmed that the crack bifurcation
 706 obeys an energy criterion as it is observed that the crack bifurcation of PMMA always occurs with the energy flux
 707 into the crack tip exceeding a critical value. Mandal et al. [143] systematically analysed mesh convergence and length
 708 scale sensitivity in dynamic crack simulation with PFMs. Quantitative evaluation of branching angles and crack tip
 709 velocity and comparison between PFM simulation results and experimental results are provided.

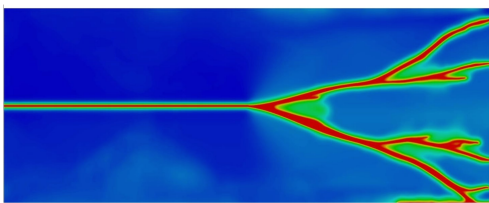


Figure 18: A 2D example of crack branching with PFMs [144].

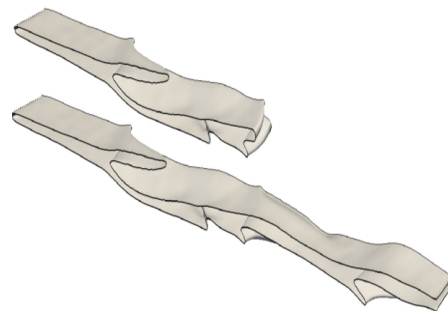


Figure 19: A 3D example of crack branching with PFMs, showing isosurfaces of phase field at $\phi = 0.3$ [145].

710 The crack branching phenomenon is very sensitive to numerical simulation parameters. For example, the solution
 711 scheme is influential, e.g. the monolithic scheme and the staggered scheme may lead to different crack patterns [146]
 712 and different branching moment [147]. The mesh size is also a significant factor, e.g. multiple crack branches can
 713 only be captured by sufficiently refined meshes while a different mesh size may result in different branching time

[131, 140, 139, 148, 147].

The sensitivity of the branching phenomenon to the mesh size leads to limitations of PFM. The computational cost will increase since the mesh needs to be fine enough for the phase field to represent the accurate position of the crack. However, PFM is a very promising model for crack branching studies with the following advantages: (1) no need for initial crack length settings and no external criteria for branching since the crack patterns can be automatically captured by solving the equation based on energy minimisation; (2) straightforward implementation in three dimensions; (3) capable of modelling multiple branches, widening of damage zone (fracture roughness) and micro-branches.

Nonlocal models/ gradient models/ viscous models. When modelling failure caused by progressive distributed damage, the material exhibits strain-softening and the governing differential equations may lose ellipticity, which renders the boundary value problem ill-posed and causes physically meaningless, mesh-dependent finite element results [149]. To solve these problems, non-local models, gradient models and viscous models are commonly employed. By introducing a characteristic length into the discretization, these models “smear” the crack over a certain domain involving several elements and avoid representing the crack topology and crack tracking algorithms [91].

An integral-type nonlocal model is defined as a model in which the constitutive law at a point of a continuum involves weighted averages of a state variable over a certain neighborhood of that point [89]. The integral formulation in the model allows the introduction of a characteristic length that qualifies the neighborhood over which the parameters/calculated numbers get “smeared” over. The gradient models can be constructed by including higher-order gradients directly in the damage loading function [150]. The higher-order gradients can be employed to smooth the non-uniformity or singularities in the strain field when regularisation of singularities or discontinuities is required. The viscosity models can be regarded as introducing higher-order time derivatives and a length scale associated with the viscosity is employed, which also restore the well-posedness of the BVP or initial BVP [91]. Detailed explanations of these models are given in literature [89, 90, 91], here we mainly focus on the performance of these models in modelling and investigating dynamic crack branching.

Examples for the application of nonlocal models and gradient models to dynamic crack branching problems can be found in [151, 152]. With an integral-type nonlocal continuum damage model, Wolff et al. [151] conducted simulations of dynamic crack branching in PMMA and studied the dynamic crack branching instabilities. It is found that the selection of the rate-dependence damage law and the critical strain for damage initiation are necessary to predict crack patterns, crack tip velocities and dissipated energies accurately. A figure of crack branching with the integral-type nonlocal continuum damage model is shown in Fig. 20. It can be observed that just like PFM, the nonlocal models are also capable of capturing the multiple branches, widening of damage zone (fracture roughness) and micro-branches. Wang et al. [152] proposed a localizing gradient damage model with micro inertia effect for modelling dynamic fracture propagation in quasi-brittle materials, which resolves the mesh sensitivity issue and spurious damage growth appeared in conventional gradient damage models and shows good performance in reproducing crack patterns (from a straight crack to sub-branching, and finally to macro branching), crack velocities, and fracture energies observed in the experiments.

The advantages of the nonlocal models, gradient models and viscous models are manifold: (1) representation of the crack topology and crack tracking algorithms are avoided; (2) the issue of mesh dependency and additional criteria to control crack branching are avoided; (3) they are capable of modelling crack surface roughness and micro-branches. Their limitations lie in that (1) physical inconsistencies may appear in the characterization of crack kinematics due to the wrong selection of related parameters, e.g. parameters for rate-dependence damage law; (2) computational cost may significantly increase due to the increase of mesh density to get a more accurate prediction of the crack.

4.2. Numerical methods

Numerical methods are employed to solve the equations of the bulk material. According to whether spatial derivatives are employed or not, the numerical methods can be further classified into continuum methods and discontinuum methods. The simulation of crack branching is a highly challenging problem due to its complexity. Difficulties if classified according to the simulation process are divided into three aspects: pre-branching, during branching and post branching. In pre-branching moving singularities at the tips of cracks should be treated accurately and a branching criterion should be detected to decide the branching time for a crack [153]. During branching a criterion or a mechanism is required to predict the crack path, including the branching patterns and branching angles. In post-branching,

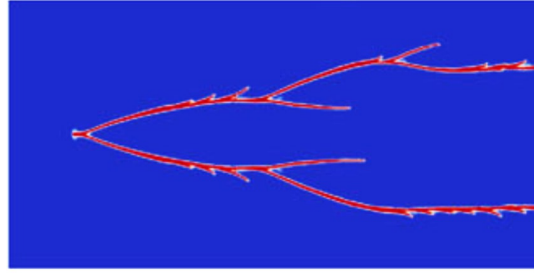


Figure 20: A numerical example of crack branching with nonlocal models [151].

764 the redistribution of energy and the influence of different branches need consideration. Until now, numerous methods
 765 have been applied to the modelling of crack branching with varying success. A superior method should have the
 766 following characteristics to better capture the phenomenon of crack branching:

- 767 • The ability of capturing different crack branching patterns, including macro crack bifurcation, micro-branches,
 768 a single crack with multiple branches and multiple cracks with branches.
- 769 • Good agreement with the experimental results and theoretical prediction in branching features, such as branch-
 770 ing angles and the crack velocity.
- 771 • Relatively easy and robust implementation process with affordable computational cost.

772 Specifically from the view of crack branching, this section summarises and compares different numerical meth-
 773 ods. For each method, the physical and mathematical principles are first introduced, followed by the explanation of
 774 crack branching simulation, after which historical and state-of-the-art applications in crack branching simulation are
 775 summarized with discussions of both advantages and limitations, see Table. 3. The emphasis differs in applications
 776 of different methods, for example, focusing more on verification (using various branching examples to prove the su-
 777 periority of the models built by the improved numerical methods) or focusing more on the analysis (analysing the
 778 mechanism behind the crack branching phenomenon with these models).

Table 3: Numerical methods for crack branching simulation.

Numerical Methods	Advantages	Limitations
FEM	flexible and robust	remeshing is required if the adaptive FEM-based model is used, which is difficult in 3D
XFEM	independent of mesh	needs special enrichment for junctions and branches
BEM	reduces dimensions	not well-suited for nonlinear problems
MMs	eliminate difficulties mesh-based methods brings	have boundary implementation, instability, numerical integration of the weak form, high computational cost issue
PD	avoids remeshing	has relatively high computational cost and difficulties in dealing with boundary conditions
DEM	well-suited when considering heterogeneity	limited in granular materials, awkward in predicting macroscopic properties and has relatively high computational cost

779 4.2.1. The continuum methods

780 *The finite element method.* The idea behind the finite element method (FEM) is to break the continuum into a number
781 of simple geometric elements and estimate the characteristics of the continuous domain by assembling the similar
782 properties of discretised elements per node [154]. The method is suitable for modelling bulk materials. It has been
783 applied to a wide range of crack problems [155] and can be combined with nearly any crack model due to its flexibility
784 and robustness, see Fig. 7.

785 In this section, depending on how the branching is simulated, a commonly used adaptive FEM-based model (FEM
786 combined with remeshing models) is discussed. Note that the term “adaptive FEM-based model” in this section does
787 not include the models based on both finite element method and cohesive elements, which are discussed in § 4.1.
788 The simulation process of crack branching using the adaptive FEM-based model mainly includes the establishment
789 and solution of the deformation equation, the selection of the propagation criterion, and the meshing strategy. By
790 establishing and solving the deformation equation, the crack footprint can be obtained. Since the crack branching
791 process is dynamic, the inertial force and the acceleration terms need to be considered. Here the Newmark method
792 [156] is used to solve the governing equations and the resulting system is given below:

$$793 (a_0\mathbf{M} + \mathbf{K})\{\mathbf{u}\}^{n+1} = \{\mathbf{F}\}^{n+1} + \mathbf{M}(a_0\{\mathbf{u}\}^n + a_2\{\dot{\mathbf{u}}\}^n + a_3\{\ddot{\mathbf{u}}\}^n) \quad (14)$$

$$794 \{\ddot{\mathbf{u}}\}^{n+1} = a_0(\{\mathbf{u}\}^{n+1} - \{\mathbf{u}\}^n) - a_2\{\dot{\mathbf{u}}\}^n - a_3\{\ddot{\mathbf{u}}\}^n \quad (15)$$

$$\{\dot{\mathbf{u}}\}^{n+1} = \{\dot{\mathbf{u}}\}^n + a_6\{\ddot{\mathbf{u}}\}^n + a_7\{\ddot{\mathbf{u}}\}^{n+1} \quad (16)$$

795 where $\{\ddot{\mathbf{u}}\}$, $\{\dot{\mathbf{u}}\}$, $\{\mathbf{u}\}$, $\{\mathbf{F}\}$ are the global vectors of nodal acceleration, nodal velocity, nodal displacement and nodal load,
796 respectively; the superscript n represents time step, \mathbf{M} and \mathbf{K} are the mass matrix and the stiffness matrix, respectively.
797 The coefficients $a_0 - a_7$ are the parameters in the Newmark method [2].

798 The next step is to determine whether the crack will branch or not. The branching criterion for the adaptive
799 FEM-based model can only be an external criterion (see § 3.2.1), which increases the difficulty of the simulation.
800 The branching time, the branching angle and the branching velocity need to be determined. Due to the singularity of
801 the crack tip, determination of appropriate physical mechanisms and formula to calculate the associated parameters
802 remains a challenge.

803 After obtaining the crack footprint, the mesh needs to be updated. It is possible to model one or two branches, but
804 as more branches develop, remeshing becomes very complex. Both the singularity at the crack tip and the small angle
805 between crack branches require a heavily refined mesh and may result in a large increase in computational cost.

806 To the best of the authors' knowledge, there do not appear to be many examples using the adaptive FEM-based
807 model to simulate crack branching due to its implementation complexity. Nishioka et al. [2] modelled the dynamic
808 crack branching phenomenon with a moving FEM (adaptive meshes) based on Delaunay triangulation and a switch-
809 ing method using the dynamic J -integral. The moving FEM has the advantage of exactly satisfying the boundary
810 conditions in front of and behind the propagating crack tip dynamically. The switching method using the dynamic
811 J -integral provides an accurate way of evaluating the dynamic J -integral regardless of crack path, which is especially
812 applicable when the crack tips are very close to each other after branching. The generation of dynamic crack branch-
813 ing phenomenon in Homalite-911 is successfully modelled and the numerical results agree well with experiments
814 [2]. However, only examples for a crack with two branches are presented and for more complicated crack branching
815 patterns are not discussed. Using a further developed remeshing strategy, Tchouikov et al. [66] investigated more
816 complicated crack branching problems including multiple crack bifurcation. A comparison between numerical and
817 experimental results was provided but the calculation efficiency was not mentioned. We conclude that the adaptive
818 FEM-based model still faces challenges when dealing with crack branching as discussed above, especially in three
819 dimensions.

820 *The extended finite element method.* In order to solve mesh dependency problems, the extended finite element method
821 (XFEM) was developed [84, 85]. Similar to FEM, it is suitable for modelling bulk materials. To simulate crack prop-
822 agation, XFEM uses the enriched shape function with discontinuous features to represent the discontinuity [157]. By
823 doing so, the displacement discontinuity can be captured and the crack can propagate on any surface within one ele-
824 ment instead of along element boundaries. Thus, remeshing and mesh dependency issues appearing in discontinuous
825 problems with FEM can be overcome. However, the use of enrichment functions also brings the issue of incompat-
826 ibility between accuracy of the solution and conditioning of the system matrix, especially when solving large 3-D

827 problems. The condition numbers of the stiffness matrix can be worse if one utilizes enrichment functions, and thus it
 828 can affect the accuracy of the solution. Several studies have attempted addressing this issue [158, 159, 160].

829 Generally, there are two ways to enrich an approximation: intrinsic enrichment (enriching the basis vector) and
 830 extrinsic enrichment (enriching the approximation) [161]. The idea for intrinsic enrichment is to enhance the approx-
 831 imation space by building new basis functions which are derived from a specific problem into the standard approxi-
 832 mation space. For instance, the asymptotic near tip displacement field can be built into the basis functions so that the
 833 singularities at the crack tip can be represented. For extrinsic enrichment, the enrichment functions are added to the
 834 standard approximation in specific zones, and as a result, the computational cost is reduced.

835 Though the characteristic of XFEM facilitates its application in modelling internal or external boundaries such
 836 as holes, inclusions, or cracks, the simulation process of crack branching with XFEM is not an easy task. First,
 837 appropriate enrichment schemes need to be considered for the element with the crack branch junctions and crack
 838 branches. Secondly, though the computational cost is less expensive without remeshing, the simulation process still
 839 requires external branching criteria, bringing issues such as the decision of reliable criteria and the calculation of
 840 related crack parameters. Thirdly, XFEM typically uses the level set method to track fractures, but as fracture branches
 841 increase the associated operation becomes increasingly complicated, especially in 3D cases. In the context of the crack
 842 branching problem, the displacement approximation \mathbf{u}^h with the partition of unity is expressed as [162]:

$$\mathbf{u}^h(\mathbf{x}) = \sum_{i \in N} \mathbf{u}_i N_i + \sum_{j \in N^H} \alpha_j N_j H(\mathbf{x}) + \sum_{k \in N^C} N_k \left(\sum_{\alpha=1}^4 \alpha_k^\alpha \Phi_\alpha \right) + \sum_{m \in N^J} \alpha_m N_m J(\mathbf{x}) \quad (17)$$

843 where \mathbf{u}_i is the vector, N_i , N_j , N_k and N_m are the standard finite element shape functions associated with node i , j ,
 844 k and m respectively; α_j , α_k^α and α_m represent the nodal enriched degrees of freedom associated with the Heaviside
 845 function $H(\mathbf{x})$, near tip asymptotic field function Φ_α and junction function $J(\mathbf{x})$, respectively; N^H , N^C and N^J are the
 846 set of nodes to enrich for the crack, crack tip and junction.

847 Progress has been made on modelling the crack branching with XFEM. Daux et al. [162] developed a method-
 848 ology to construct the enriched approximation based on the interaction of the discontinuous geometric features and
 849 calculated the SIF of static cracks with multiple branches. This can be used for static cracks, but the propagation of
 850 the dynamic crack branching process is not taken into consideration. To improve the modelling of dynamic crack
 851 propagation by XFEM, Belytschko et al. [163] developed a new methodology for treating elements that contain crack
 852 tips, which allows the velocity field of the element containing the crack tip can change smoothly from a partially cut
 853 element to a fully cut element. The crack path and velocity can be determined directly by the loss of hyperbolicity
 854 criterion, which facilitates the modelling of dynamic crack growth problems, including crack branching. However,
 855 only a relatively simple bifurcation phenomenon is captured, while fracture roughness and micro-branches can not be
 856 captured, see Fig. 21. To seize the discontinuity around the junction of a branched crack, Xu et al. [58] introduced the
 857 enrich scheme of the element crossed by two separated cracks, the element embedded by a junction, and the way of
 858 constructing the diagonal mass matrix for the branched element, with which the initial branching process of a moving
 859 crack (the main crack develops two branches) is successfully simulated. However, this method requires an increase
 860 in additional degrees of freedom. For more complex branching problems with increasing degrees of freedom in one
 861 element, Chen and Zhou [164] proposed an enhanced XFEM coupling the phantom node method [165] and proved
 862 its robustness and accuracy in handling the complex branched crack problems. To capture complicated discontinuity
 863 patterns, Song and Belytschko [166] introduced a hybrid discontinuity tracking-fitting method that fits cracks with
 864 discrete discontinuities at nodes based on the XFEM. This method is quite similar to the cracking particles method,
 865 which is capable of modelling complicated fracture patterns since it needs no explicit representation of the crack's
 866 topology.

867 In summary, the XFEM possesses the following advantages: (1) lower computational cost without the need of
 868 remeshing; (2) suitable for cracks with complex geometry or problems with geometric nonlinearities because of
 869 mesh independence. These advantages make the XFEM become a powerful and promising tool in the simulation of
 870 complex crack problems. However, the XFEM has imitations when dealing with multiple interacting and branched
 871 cracks and micro-branches, since the computational cost increases as the number of cracks grows and its formulation
 872 becomes increasingly complex. For branches or junctions, special discontinuous displacement enrichment needs to
 873 be developed and external criteria for the injection of the enrichment are needed. Additionally, because of the lack of
 874 a reliable crack branching criterion, prediction of crack propagation and branching remains a challenge [91].

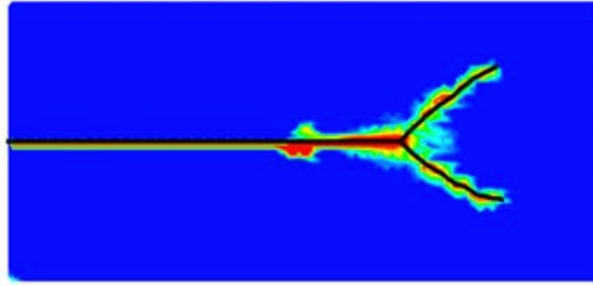


Figure 21: A numerical example of damage for crack branching with XFEM [163].

875 *The boundary element method.* The boundary element method (BEM) is also widely used in crack simulations due
 876 to its ability to automatically follow the propagation of the crack with limited remeshing and its inherent accuracy
 877 [167]. The BEM is designed for solving boundary value or initial value problems and formulated in terms of boundary
 878 integral equations [168]. Similar to the FEM, the BEM is suitable for modelling bulk materials. Instead of discretising
 879 the whole domain into volume elements, the BEM only discretises the domain boundary for interpolation approxima-
 880 tion. The basic process of modelling crack propagation with BEM is slightly different from FEM. The mathematical
 881 model needs to be established first, then the boundary integral equations can be obtained by taking boundary values
 882 in the representation formula. After generating the system of discrete equations by collocation, Galerkin's method or
 883 the least squares method, the displacement field can be solved. During this process, crack parameters related to the
 884 external propagation criteria, such as stress intensity factor and energy release rate, need to be calculated to determine
 885 crack development. The calculation of these parameters is much simpler than FEM due to the reduced dimensional
 886 features of BEM. Once the crack develops, remeshing is needed by adding the elements at the end of the crack tip
 887 without changing the remaining mesh.

888 The displacement integral equation at an interior point \mathbf{X} in the absence of a body force for linear elastic crack
 889 problems is given by [167]:

$$\mathbf{u}_i(\mathbf{X}) = \int_{\Gamma_S + \Gamma_n^+ + \Gamma_n^-} \mathbf{U}_{ij}(\mathbf{X}, \mathbf{x}) \cdot \mathbf{t}_j(\mathbf{x}) d\Gamma - \int_{\Gamma_S + \Gamma_n^+ + \Gamma_n^-} \mathbf{T}_{ij}(\mathbf{X}, \mathbf{x}) \cdot \mathbf{u}_j(\mathbf{x}) d\Gamma \quad (18)$$

890 where Γ_n^+ and Γ_n^- represent the upper and lower crack surfaces, respectively, and Γ_S represents the outer boundary, \mathbf{u}_j
 891 and \mathbf{t}_j denote the boundary displacement and the traction, respectively; \mathbf{U}_{ij} and \mathbf{T}_{ij} are the fundamental solutions for
 892 displacement and traction, respectively. Fig. 22 shows a schematic illustration of crack branching simulated by BEM.

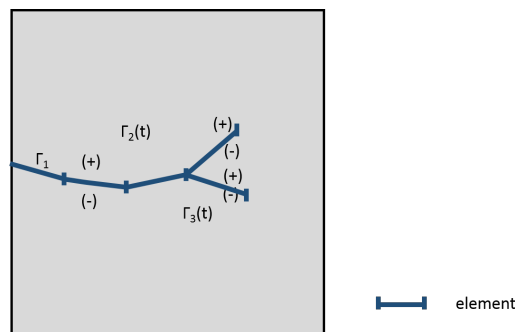


Figure 22: A schematic illustration of crack branching with BEM.

893 The difficulties of BEM for fracture problems reside in the coincidence of crack nodes, giving rise to a singu-
 894 lar system of algebraic equations. Different techniques such as the sub-region boundary element method (SBEM),
 895 displacement discontinuity methods (DDM), dual-boundary element method (DBEM) and dual-reciprocity boundary
 896 element method have been developed to solve this problem [92]. Seelig and Gross [169] presented a pioneering work

897 of modelling dynamic crack branching with BEM, where crack growth and branching criteria were combined and
898 a time-domain boundary integral equation system was established. The crack propagation speed and the SIF were
899 calculated, showing good agreement with the experimental observations. Since then, examples for BEM simulation
900 of crack branching have been presented in the literature [64, 170, 171, 172, 173, 174, 175].

901 Branching examples are used to verify the improvement and accuracy of the proposed schemes. For example,
902 Rajapakse and Xu [170] presented a complete set of piezoelectric Green's functions in closed form and developed
903 a solution scheme based on the boundary integral equation method to analyse plane cracks in piezoelectric solid.
904 A double-branched crack model is used to verify this scheme. Yan [171] tried to place the crack-tip displacement
905 discontinuity elements at the corresponding crack tip on top of the constant displacement discontinuity elements that
906 cover the entire crack surface. By using such elements and the SIF as a propagation criterion with a known branching
907 angle, complex crack problems including a branched crack example are employed to demonstrate the efficiency and
908 accuracy of the proposed method. Santana and Portela [173] applied the dual boundary element method (DBEM) to
909 the analysis of mixed-mode multiple-crack growth including branching cracks, where the SIF was evaluated via the J -
910 integral and the incremental analysis was used to define the direction and the extension of multiple interacting cracks.
911 Other approaches focus on the study of the physical mechanisms behind the branching phenomenon. Rafiee et al.
912 [64] investigated fast running cracks branching under different bi-axial loading conditions. It is found that branching
913 depends on the opening mode SIF, the crack velocity, and the orientation on the maximum circumferential stress in
914 the vicinity of the crack tip. Marji [172] modelled the crack branching process by using an indirect BEM specially
915 developed to treat the kink points of propagating cracks in brittle solids and studied the mechanism of secondary crack
916 initiation and propagation. The results show that the formation of the wing crack and the secondary crack caused by
917 the crack tip and the crack kink point may lead to a quasi-static crack bifurcation process. Fedelinski [174] applied the
918 BEM to the analysis of the branched and intersecting cracks in statically and dynamically loaded plates. The influences
919 of angles between branches of the crack and dimensions of the plate for the star-shaped crack on a dynamic SIF
920 were analysed. Shrivastava et al. [175] presented a hydraulic fracture model with a three-dimensional displacement
921 discontinuity method and investigated the interaction between multiple cracks and branches. The heterogeneity of
922 solid rocks is one reason for crack branches, which further results in a complex fracture network.

923 The BEM offers clear advantages. The stress field in the vicinity of the crack tip can be accurately calculated
924 and the computational efficiency can be greatly increased due to the reduction of the dimension. Nevertheless, it
925 still suffers from the inability to model crack propagation and branching autonomously as it needs external criteria.
926 Besides, the application of BEM in nonlinear problems is limited, as it still requires that the fundamental solution is
927 expressed in terms of Green's functions [91].

928 *The meshfree methods.* When dealing with crack branching problems, the traditional FEM has the limitation of
929 remeshing, which is time-consuming especially in 3D. The XFEM avoids the need of remeshing, however, it is
930 awkward when dealing with multiple interacting and branched cracks, since the computational cost increases as
931 the number of cracks grows and its formulation becomes increasingly complex. Meshfree methods (MMs) were
932 devised with the objective of eliminating part of the difficulties associated with reliance on a mesh to construct the
933 approximation [176], providing an advantage in dealing with crack growth problems.

934 In general, MMs refer to numerical techniques that do not require any predefined mesh information for domain
935 discretization, and they use a set of points scattered within the problem domain as well as on the boundaries of the
936 domain to represent the problem domain and its boundaries [177]. MMs model the bulk material as continuum.
937 Approaches of modelling discontinuities in MMs can be classified into two types generally: methods based on the
938 intrinsic and extrinsic enrichment and modification of the weight function [176]. The second type can be further
939 classified into the visibility method, the diffraction method, the transparency method, and the “see through” and
940 “continuous line” method [86]. Pioneered by Gingold and Monaghan [178], the smoothed particle hydrodynamics
941 method (SPH) was developed on a strong form, while other methods were developed later based on a weak form,
942 among which the element-free Galerkin method (EFGM), reproducing kernel particle method (RKPM), material point
943 method (MPM) are popular approaches [177]. Compared with MMs based on strong forms, the MMs based on
944 weak forms are more robust and steady. Detailed descriptions of these MMs and their classifications, advantages,
945 limitations, and computer implementation aspects can be found in studies by [86, 91, 176, 179, 180, 181]. Here, we
946 only give a brief introduction of these MMs and focus more on their ability of capturing crack branching.

947 SPH is a pure Lagrangian, meshfree method, which was first developed to model hydrodynamic flows and then

948 extended to solid mechanics [182, 183]. In SPH, the domain is discretised into particles and each particle interacts
949 with its neighbour particles within its influence domain through a kernel function. Early works on studying crack
950 with SPH can be found in [184, 185, 186, 187]. In most of these work, the SPH is based on Eulerian kernels (kernel
951 functions which are expressed in terms of spatial coordinates) and the crack can occur naturally due to separating
952 particles. Compared with the traditional mesh-based methods, it avoids the mesh dependence problem when dealing
953 with cracks. However, it suffers from problems such as spurious instabilities, expensive computational cost and
954 inaccurate crack path prediction [188, 176]. To solve these problems, Lagrangian kernels (kernel functions in terms
955 of material coordinates) instead of Eulerian kernel functions are employed [189, 190]. However, Lagrangian kernels
956 require specific strategies to deal with fractures since neighbour particles do not change during a simulation. A
957 commonly used strategy is the visibility method, in which the displacement discontinuity is modelled by excluding
958 the particles on the opposite side of the crack in the approximation of the displacement field under the assumption of
959 opaque crack boundary [86]. Recently, a strategy called “pseudo-spring” was developed by Chakraborty and Shaw
960 [191] to facilitate SPH to model crack propagation without any numerical artefact. The crack path can be tracked
961 automatically by the broken pseudo-springs. Using the Pseudo-Spring smoothed particle hydrodynamics method
962 (Pseudo-Spring SPH), Islam and Shaw [192] simulated 2D and 3D crack propagation and branching and studied
963 effects of tensile loading amplitude on crack branching.

964 The element free Galerkin methods (EFG), first developed by [193], is a method based on moving least-square
965 (MLS) interpolants. The EFG requires only nodal data without the requirement of element connectivity. Compared
966 with SPH, the EFG avoids the calculation of nodal volumes and obtains the gradient fields directly by taking the
967 derivatives of the interpolants with respect to spatial variables, which increases the accuracy and stability [193]. This
968 feature makes it quite suitable for static and dynamic crack problems. Rabczuk and Areias [194], Rabczuk and Zi
969 [97] proposed the extended element free Galerkin (XEFG) method for cohesive crack initiation, propagation and
970 branching in two and three-dimensional statics and dynamics. However, the closure of the crack along the front
971 is ensured through near-tip enrichment, which leads to the difficult selection of near-tip enrichment fields in large
972 strain or non-linear materials. To simulate crack propagation in non-linear solids including large deformations, Zi
973 et al. [195] proposed an XEFG method which closes the crack tip without near-tip enrichment. The entire crack
974 is enriched by the sign function. The domain-decrease method is used to remove the branch enrichment from the
975 discontinuous displacement field. The method is successfully applied to crack branching problems in 2D and the
976 results agree well with the experiment results, see Fig. 23. Later, the method was extended to 3D by employing an
977 extrinsic discontinuous enrichment and adding a Lagrange multiplier field along the crack front to close the crack
978 by Bordas et al. [196]. In this way, the computational cost was further decreased. The method proved to be capable
979 of modelling initiation, branching, growth and coalescence of an arbitrary number of cracks in non-linear solids by
980 different benchmark examples. Fig. 24 shows the branching example provided in [196], which is a “2.5D” example
981 rather than a real 3D example. The ability of the method for simulation of real 3D crack growth is demonstrated
982 by another example of a circular-cylindrical chalk bar under torsion, which is not shown here since this example
983 does not include the crack branching phenomenon. Rabczuk et al. [197] reviewed different crack tracking techniques
984 in three-dimensions applicable in the context of partition of unity methods, especially meshfree methods. A crack
985 tracking procedure is proposed and implemented in the context of XEFG and two possibilities for crack closure are
986 presented: crack closure by crack front enrichments and crack closure without crack front enrichment by use of
987 Lagrange multipliers. Three-dimensional crack branching examples were given and showed good agreement with the
988 results from the literature [75].

989 To develop more accurate and efficient mesh-free interpolation functions, the reproducing kernel particle method
990 (RKPM) was introduced as an improvement of the continuous SPH approximation by Liu et al. [198]. It maintains
991 the advantages of SPH, however, because of the addition of a correction function, it gives much more accurate results.
992 Guan et al. [199] studied the dynamic failure and fragmentation with a semi-Lagrangian RKPM, which successfully
993 alleviated mesh distortion difficulties associated with the Lagrangian FEM. Klein et al. [200] used the virtual internal
994 bond model with RKPM to model the propagation of cohesive cracks. The model demonstrates its capabilities of
995 predicting the onset of crack path instabilities. With the model, simulations of crack tip instabilities and branching are
996 conducted and theoretical analysis of branching is given.

997 The material point method (MPM) is a quasi-particle method introduced by Sulsky et al. [201]. In the MPM, a
998 continuum body is described into a number of material points, which carry all the information of material properties.
999 The material points are surrounded by a background mesh, which is used only to solve the governing equations.

1000 In each time step, the parameters and variables are transferred back and forth between material points and grids
 1001 [202]. The MPM successfully eliminates the disadvantages of numerical difficulties associated with mesh distortion
 1002 in Lagrangian and with the advected quantities in Eulerian description [203]. Some examples of the accurate and
 1003 effective simulation of fracture propagation with MPM can be found in [204, 205, 206, 207, 208]. However, only one
 1004 of them simulates and studies the crack branching phenomenon [208], where a phase field MPM is introduced for
 1005 robust simulation of dynamic fracture in elastic media considering the anisotropic surface energy. With the model,
 1006 the influence of surface energy anisotropy and loading conditions on crack patterns including crack branching are
 1007 evaluated.

1008 The MMs eliminate difficulties of mesh-based methods, such as mesh generation problems for complex 3D mod-
 1009 els, accuracy problems due to distorted or low quality meshes, adaptive remeshing resulting from dynamic problems.
 1010 However, they still suffer from implementation of boundary conditions, high computational cost, instability and in-
 1011 consistency problems. In addition, when modelling crack branching, crack surfaces representation and crack tracking
 1012 algorithms are usually required, which introduces additional challenges associated with the numerical integration of
 1013 the weak form through tracking complex crack geometry, especially for tracking complex 3D crack geometry.

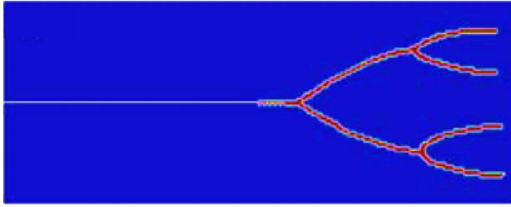


Figure 23: A 2D example of crack branching with MMs [195].

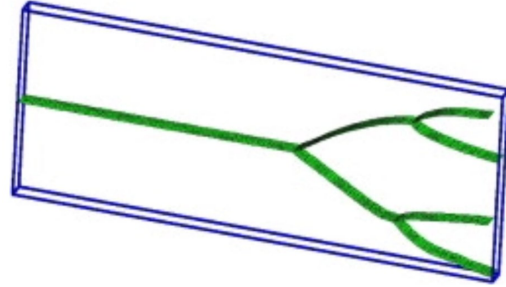


Figure 24: A 3D example of crack branching with MMs [196].

1014 4.2.2. The discontinuum methods

1015 *The peridynamics.* Peridynamics (PD) is a new continuum mechanics formulation originally developed by Silling
 1016 [209] in 2000. By replacing the partial differential equation with the integral equation, PD avoids the singularity and
 1017 combines continuous and discontinuous descriptions together, which makes it a promising tool for the study of crack
 1018 problems. There are two types of theoretical models for PD: the bond-based PD and the state-based PD. The bond-
 1019 based PD assumes that any pair of particles interact only through a central potential that is totally independent of all
 1020 other local conditions [78]. This assumption results in that for an isotropic, linear, microelastic material, the Poisson's
 1021 ratio is limited to 1/4 (plain strain) or 1/3 (plane stress), which makes the bond-based PD not well suited to model
 1022 complex material behaviour reliable. To remove the restrictions for Poisson's ratio, Silling et al. [210] proposed the
 1023 state-based PD. In the state-based PD, the interaction between two material points depends both on the bond between
 1024 the two points and the deformation of all the other bonds in the horizon. The state-based PD can be further divided
 1025 into the ordinary state-based PD and non-ordinary state-based PD. Here, the bond-based PD is given as an example
 1026 for simplicity to further explain the crack simulation process.

1027 In PD, a material medium is treated as a composition of individual material points [209]. Each material point \mathbf{x} is
 1028 assumed to interact with the other material points \mathbf{x}' around it within a local region \mathcal{H} , which is referred as "horizon".
 1029 With a volume of V and mass density ρ , the material point is identified by its coordinates \mathbf{x} in the initial configuration.
 1030 The bond-based PD equation of motion at a reference position \mathbf{x} and time t is given as [209]:

$$\rho(\mathbf{x})\ddot{\mathbf{u}}(\mathbf{x}, t) = \int_{\mathcal{H}} \mathbf{f}(\mathbf{x}' - \mathbf{x}, \mathbf{u}' - \mathbf{u})dV + \mathbf{b}(\mathbf{x}, t) \quad (19)$$

1031 where \mathbf{x} and \mathbf{x}' represent the position vectors of the material point in initial configuration, $\ddot{\mathbf{u}}$ is the acceleration vector
 1032 of material point \mathbf{x} at time t , \mathbf{u} and \mathbf{u}' are the displacement of material points \mathbf{x} and \mathbf{x}' , respectively, \mathbf{b} is a prescribed
 1033 body-force density field, \mathbf{f} is the pairwise force defined as the force per unit volume squared between two material

1034 points \mathbf{x} and \mathbf{x}' :

$$\mathbf{f} = c s \frac{\mathbf{y}' - \mathbf{y}}{|\mathbf{y}' - \mathbf{y}|} \quad (20)$$

1035 in which \mathbf{y} and \mathbf{y}' represent the position vectors of the material point \mathbf{x} and \mathbf{x}' in the deformed configuration, respec-
 1036 tively. c is the PD material parameter and is referred to as the bond-constant and the stretch s between the material
 1037 points is defined as

$$s = \frac{|\mathbf{y}' - \mathbf{y}| - |\mathbf{x}' - \mathbf{x}|}{|\mathbf{x}' - \mathbf{x}|} \quad (21)$$

1038 No complex criteria are needed during the simulation process for crack initiation and propagation as the crack
 1039 growth can occur spontaneously with only one bond-break (interactions) criterion. A simple criterion for a bond-
 1040 break is that if the elongation of a bond is greater than a given threshold, the bond breaks and cannot be recovered.
 1041 The time taken by the bond-break is completely determined by the material geometry and loading conditions. When
 1042 a series of bonds break, the discontinuous space formed by these broken bonds becomes a macroscopic crack. A
 1043 variable (value between 0-1, 1 represents total failure while 0 represents no failure) is often employed to define the
 1044 local damage at each point, thus, the crack path can be indicated by plotting the local damage.

1045 Due to its intrinsic features, the PD also has the advantages of avoiding complex fracture criteria and remeshing.
 1046 Applications of PD for crack branching are discussed from three perspectives in the following paragraphs.

1047 First, by employing or improving the PD, demonstration of capturing complex crack patterns with crack branching
 1048 and multiple crack branches examples is given. Ren et al. [211] proposed the dual-horizon peridynamic formulation,
 1049 which naturally includes varying horizon sizes and completely solves the “ghost force” issue [212, 213]. Zhou et al.
 1050 [214] proposed the extended non-ordinary state-based PD, where the stress-based failure criteria are implemented.
 1051 The breakage of bonds is determined by the mean stresses between the interacting material points rather than the
 1052 stretch of bonds. Dipasquale et al. [215] proposed adaptive refinement algorithms for 2D peridynamic grids and as a
 1053 consequence, computational resources are efficiently employed. All of the PD methods above select crack branching
 1054 examples to prove their capability.

1055 Secondly, after demonstrating the ability of capturing complex crack patterns, the PD is applied to capture var-
 1056 ious branching phenomena, including crack surface roughening, successive branching, micro-branches and multiple
 1057 branches. Then numerical results from PD are compared with numerical results from other methods or results from
 1058 experiments and theories. Ha and Bobaru [216] found that before branching the damage zone becomes thicker through
 1059 PD simulation, which is similar to the roughening before branching observed in the experiments. Later, Ha and Bo-
 1060 baru [217] found that the PD model captures experimentally observed successive branching events and secondary
 1061 cracking. It is found by Agwai et al. [113] that the PD simulation can capture small branches in the glass plate before
 1062 the crack splits into two main branches. The micro-branches are in good agreement with experimental results. Bobaru
 1063 and Zhang [218] observed that as loading increases, multiple branches are observed in soda-lime glass under stress
 1064 on boundaries, see Fig. 25. From the figure, multiple branches and the widening of damage zone before branching
 1065 can be observed. With a 3D PD model, Butt and Meschke [219] simulated a local crack front bifurcation grow into
 1066 a micro-branch, which arrests soon or grows into a macro-branch. Distinct features on the crack surface due to the
 1067 localized bifurcations and micro-branches are also captured with the model, known as “mirror”, “mist” and “hackle”
 1068 fracture surfaces in experimental observations [14], see Fig. 26.

1069 Thirdly, through the observation of various phenomena, influencing factors and the mechanisms of crack branching
 1070 are discussed and analysed. Ha and Bobaru [216] summarized that reflecting stress waves from the boundaries have
 1071 a strong influence on the shape and structure of the crack paths in dynamic fractures. Later, Bobaru and Hu [220]
 1072 explained why in the simulation of [216] the propagation velocity of a dynamic crack is influenced by the horizon
 1073 size. This is because the crack propagation velocity, crack branching angles and branching time are independent
 1074 of the horizon size only in the condition that the fracture process does not interact with the stress waves. Chen
 1075 et al. [221] assumed that the branching moment and velocity are very sensitive to the micro-modulus function as the
 1076 branching velocity after the first branching moment can slightly increase or decrease or stay constant under various
 1077 micro-modulus functions. Through PD simulations under various conditions, Bobaru and Zhang [218] proposed that
 1078 stress waves pile up around the crack tip and lead to “migration” of damage sufficiently large, thus the material in
 1079 front of the original crack tip becomes relaxed and the crack branching ensues. Butt and Meschke [219] explained the

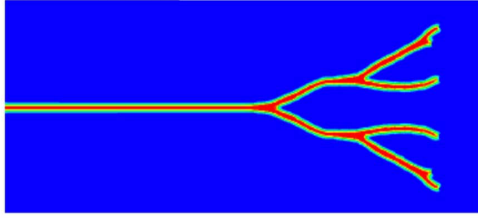


Figure 25: A 2D example of crack branching with PD [218].

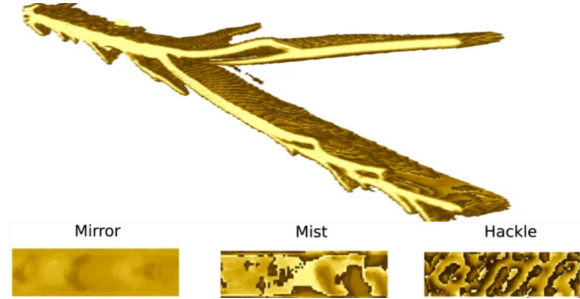


Figure 26: A 3D example of crack branching with PD [219].

1080 influence of PD horizon, dimensionality and specimen size on dynamic fracture propagation with PD analysis. All of
 1081 them have an influence on the crack branching patterns.

1082 Generally speaking, the PD has been observed to perform well in modelling branching problems by circumventing
 1083 difficulties in remeshing and the requirement of an external branching criterion. In addition, it has the ability of
 1084 modelling multiple branches, widening of damage zone (fracture roughness) and micro-branches. However, more
 1085 research is required to improve existing PD methods for better computational efficiency compared with traditional
 1086 methods such as FEM. Though the remeshing process in FEM is eliminated, they introduce additional challenge
 1087 associated with the numerical integration through tracking complex 3D crack geometry/surfaces. In addition, as a
 1088 nonlocal method, the implementation of boundary conditions needs to be considered.

1089 *The discrete element method.* Originally developed by Cundall and Strack [222], the discrete element method (DEM)
 1090 has been used in the modelling of jointed structures and granular materials. It models the bulk material as discontinuum
 1091 and can also be applied in modelling of fracturing and fragmentation, where the discontinuities are the natural
 1092 outcome of the deformation process [223]. As a discontinuum method, the DEM treats a material medium as an
 1093 assembly of distinct particles, the motion of particles is governed by Newton's laws, and forces between particles are
 1094 calculated according to the small overlap between them. In DEM crack simulation, when the maximum stress exceeds
 1095 the tensile or shear strength, cracks initiate and propagate [92]:

$$\begin{aligned}
 F_n &= k_n u_n \\
 \Delta F_s &= k_s \Delta u_s \\
 \frac{|F_s|}{A} &\leq c_d + \frac{F_n \tan \beta}{A}
 \end{aligned}
 \tag{22}$$

1096 where F_n is the normal force, A is the area, k_n is the normal stiffness, u_n is the normal displacement, ΔF_s is the change
 1097 in shear force, k_s is the shear stiffness, Δu_s is the incremental shear displacement and c_d and β are the cohesion and
 1098 joint friction angle, respectively. An example of fracture simulation using the DEM is given in Fig. 27.

1099 DEMs can be classified with various criteria, e.g. the type of contact between bodies, the representation of
 1100 deformability of solid bodies, the methodology for detection and revision of contacts, and the solution procedure for
 1101 the equations of motion [225]. Though solution procedure for modelling crack propagation with DEM is different
 1102 with different deformability of solid bodies (the explicit and implicit one), some steps are indispensable [223]: (1)
 1103 identification of the unit (rock blocks, material particles, mechanical parts or fracture systems) system topology; (2)
 1104 formulation and solution of equations of motion of the individual units; (3) the detection and updating of varying
 1105 contacts (or connectivity) between the units as the consequences of their motions and deformations. The DEM differs
 1106 from other methods based on continuum mechanics e.g. FEM in that the contacts between units are varying with
 1107 time and deformation while remaining fixed in other methods. The DEM is most successful in modelling granular
 1108 materials. Its applications in modelling continuum materials are being explored, but have various limitations.

1109 Due to the unique nature of DEM, it can model crack branching with taking into account heterogeneities [226].
 1110 Some examples of using DEM to study the crack branching in heterogeneous materials are listed below. Taking into

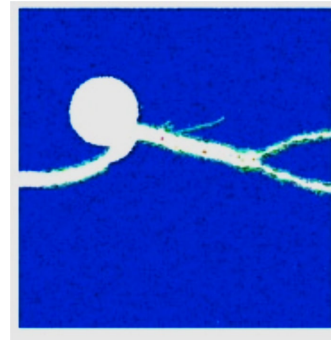
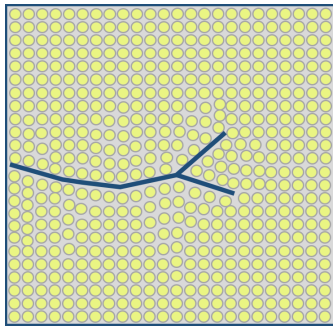


Figure 27: A schematic illustration of crack branching with DEM. Figure 28: A numerical example of crack branching with DEM [224].

1111 account the effect of local heterogeneity around the crack tip, Hedjazi et al. [224] modelled crack branching in a
 1112 vitreous biopolymer material based on DEM, see Fig. 28. A hole is set in the material to investigate the influence
 1113 of the position of the hole on crack branching patterns. The results showed that DEM is more sensitive to stress
 1114 heterogeneities and has better agreement with experimental results than FEM. Hofmann et al. [227] studied fracture
 1115 branching with a grain-based modelling approach and found that complex fracture patterns are governed by material
 1116 heterogeneity and model discretization. Chung et al. [228] used DEM to model microcracks initiation and propagation
 1117 in different crystal structures, and found that the crack branching pattern varies with different notch inclination angles:
 1118 the larger the notch inclination angle is, the more branching occurs.

1119 Though DEM can be applied in the crack branching simulation in heterogeneous materials, its limitations are very
 1120 obvious : (1) it is not well suited to model complex material behaviour reliably and its application is mostly limited to
 1121 granular materials; (2) it is awkward in predicting a variety of macroscopic properties (e.g. elastic stiffness, strength,
 1122 critical energy release rate for uni-, bi- and tri-axial loading, etc.); (3) it usually has high computational cost, which is
 1123 easily influenced by many factors, such as particle numbers, particle shapes and contact force models [223].

1124 5. Summary and Prospective Work

1125 This paper presents an overview of crack branching, including experimental observations, physics of crack branch-
 1126 ing, and crack models and numerical methods for simulation of crack branching problems. In terms of experimental
 1127 observations, high speed photography is the most commonly used technique to be combined with photoelasticity,
 1128 caustics, digital image correlation, digital gradient sensing to study the crack branching. The current focus is on (1)
 1129 how to combine and improve upon existing shortcomings with the combination of technology development; (2) how
 1130 to simplify the operations and reduce operating costs while ensuring high temporal and spatial resolution. Supported
 1131 by experimental research, physics of branching including the causes of crack branching and branching criteria have
 1132 been investigated and summarized. One explanation suggests the branching occurs once the crack velocity exceeds a
 1133 critical value (related to the wave speed). Another explanation assumes branching is a natural outcome of the growth
 1134 of microcracks near the crack tip and energy absorbed into the crack is related to the limiting velocity. Dynamic in-
 1135 stabilities, which are related to critical velocity, fracture roughness and micro-branches, are also shown to be a strong
 1136 mechanism for crack branching and are investigated. In addition, the crack front waves and the tilting and twisting of
 1137 the stress vector at the crack front are responsible for the crack branching. Corresponding to these potential causes to
 1138 crack branching, different branching criteria have been proposed, including external and internal criteria. The crack
 1139 models and numerical methods for crack branching have been developed and continuously improved according to
 1140 various crack branching criteria, which are further applied to simulate crack branching, to shed light on the mech-
 1141 anisms behind branching. These models and methods are reviewed in this paper with respect to their strengths and
 1142 limitations.

1143 Several outstanding issues and challenges are identified and need to be resolved for reliable crack branching
 1144 prediction, these include the limitation of experimental techniques for the observation and measurements of physical
 1145 parameters in front of the crack tip; current analytical techniques and existing branching criteria are not sufficient to
 1146 define the mechanisms driving crack branching and associated dynamic instabilities; the limitations of various crack

1147 models and numerical methods proposed for simulating complex fracture propagation processes. Moreover, the study
 1148 of the branching problem is further complicated by considerations such as heterogeneity of the material, softening
 1149 behaviour and large fracture networks in which multiple length scale cracks develop.

1150 Acknowledgements

1151 The authors would like to thank the supports from China Scholarship Council (CSC No.: 201709370055), Swansea
 1152 University (Zienkiewicz Scholarship), and the Royal Society (Ref.: IEC\NSFC\191628).

1153 References

- 1154 [1] Kalthoff, J.. On the propagation direction of bifurcated cracks. In: Proceedings of an international conference on Dynamic Crack Propaga-
 1155 tion. Springer; 1973, p. 449–458.
- 1156 [2] Nishioka, T., Furutuka, J., Tchouikov, S., Fujimoto, T.. Generation-phase simulation of dynamic crack bifurcation phenomenon using
 1157 moving finite element method based on delaunay automatic triangulation. *Computer modelling in Engineering and Sciences* 2002;3(1):129–
 1158 145.
- 1159 [3] Ramulu, M., Kobayashi, A.. Mechanics of crack curving and branching—a dynamic fracture analysis. *Dynamic fracture* 1985;:61–75.
- 1160 [4] Ravi-Chandar, K., Knauss, W.. An experimental investigation into dynamic fracture: Iii. on steady-state crack propagation and crack
 1161 branching. *International Journal of Fracture* 1984;26(2):141–154.
- 1162 [5] Anderson, T.L.. *Fracture mechanics: fundamentals and applications*. CRC press; 2017.
- 1163 [6] Guozden, T.M., Jagla, E.A., Marder, M.. Supersonic cracks in lattice models. *International journal of fracture* 2010;162(1-2):107–125.
- 1164 [7] Freund, L.. *Dynamic Fracture Mechanics*. Cambridge Monographs on Mechanics; Cambridge University Press; 1998.
- 1165 [8] Ravi-Chandar, K.. *Dynamic Fracture*. Elsevier Science; 2004. ISBN 9780080472553.
- 1166 [9] Schardin, H.. Velocity effects in fracture. In: *ICF0, Swampscott-MA (USA) 1959*. 1959, p. 297–330.
- 1167 [10] Kerkhof, F.. General lecture wave fractographic investigations of brittle fracture dynamics. In: Proceedings of an international conference
 1168 on Dynamic Crack Propagation. Springer; 1973, p. 3–35.
- 1169 [11] Kobayashi, A., Mall, S.. Dynamic fracture toughness of homalite-100. *Experimental Mechanics* 1978;18(1):11–18.
- 1170 [12] Dally, J.W.. Dynamic photoelastic studies of fracture. *Experimental Mechanics* 1979;19(10):349–361.
- 1171 [13] Ravi-Chandar, K., Knauss, W.. An experimental investigation into dynamic fracture: I. crack initiation and arrest. *International Journal of*
 1172 *Fracture* 1984;25(4):247–262.
- 1173 [14] Ravi-Chandar, K., Knauss, W.. An experimental investigation into dynamic fracture: Ii. microstructural aspects. *International Journal of*
 1174 *Fracture* 1984;26(1):65–80.
- 1175 [15] Ravi-Chandar, K., Knauss, W.. An experimental investigation into dynamic fracture: Iv. on the interaction of stress waves with propagating
 1176 cracks. *International Journal of Fracture* 1984;26(3):189–200.
- 1177 [16] Fineberg, J., Gross, S.P., Marder, M., Swinney, H.L.. Instability in dynamic fracture. *Physical Review Letters* 1991;67(4):457.
- 1178 [17] Fineberg, J., Gross, S.P., Marder, M., Swinney, H.L.. Instability in the propagation of fast cracks. *Physical Review B* 1992;45(10):5146.
- 1179 [18] Sharon, E., Gross, S.P., Fineberg, J.. Local crack branching as a mechanism for instability in dynamic fracture. *Physical Review Letters*
 1180 1995;74(25):5096.
- 1181 [19] Sharon, E., Fineberg, J.. Microbranching instability and the dynamic fracture of brittle materials. *Physical Review B* 1996;54(10):7128.
- 1182 [20] Sharon, E., Gross, S.P., Fineberg, J.. Energy dissipation in dynamic fracture. *Physical review letters* 1996;76(12):2117.
- 1183 [21] Fineberg, J., Marder, M.. Instability in dynamic fracture. *Physics Reports* 1999;313(1-2):1–108.
- 1184 [22] Bouchbinder, E., Livne, A., Fineberg, J.. Weakly nonlinear theory of dynamic fracture. *Physical Review Letters* 2008;101(26):264302.
- 1185 [23] Bouchbinder, E., Livne, A., Fineberg, J.. Weakly nonlinear fracture mechanics: experiments and theory. *International journal of fracture*
 1186 2010;162(1-2):3–20.
- 1187 [24] Bouchbinder, E., Goldman, T., Fineberg, J.. The dynamics of rapid fracture: instabilities, nonlinearities and length scales. *Reports on*
 1188 *Progress in Physics* 2014;77(4):046501.
- 1189 [25] Livne, A., Ben-David, O., Fineberg, J.. Oscillations in rapid fracture. *Physical review letters* 2007;98(12):124301.
- 1190 [26] Fineberg, J., Bouchbinder, E.. Recent developments in dynamic fracture: some perspectives. *International Journal of Fracture* 2015;196(1-
 1191 2):33–57.
- 1192 [27] Hawong, J., Kobayashi, A., Dadkhah, M., Kang, B.J., Ramulu, M.. Dynamic crack curving and branching under biaxial loading.
 1193 *Experimental Mechanics* 1987;27(2):146–153.
- 1194 [28] Hauch, J., Marder, M.. Energy balance in dynamic fracture, investigated by a potential drop technique. *International Journal of Fracture*
 1195 1998;90(1-2):133–151.
- 1196 [29] Suzuki, S., Sakaue, K., Iwanaga, K.. Measurement of energy release rate and energy flux of rapidly bifurcating crack in homalite 100 and
 1197 araldite b by high-speed holographic microscopy. *Journal of the Mechanics and Physics of Solids* 2007;55(7):1487–1512.
- 1198 [30] Murphy, N., Ali, M., Ivankovic, A.. Dynamic crack bifurcation in pmma. *Engineering Fracture Mechanics* 2006;73(16):2569–2587.
- 1199 [31] Fayyad, T.M., Lees, J.M.. Experimental investigation of crack propagation and crack branching in lightly reinforced concrete beams using
 1200 digital image correlation. *Engineering Fracture Mechanics* 2017;182:487–505.
- 1201 [32] Skarżyński, Ł., Tejchman, J.. Experimental investigations of fracture process using dic in plain and reinforced concrete beams under
 1202 bending. *Strain* 2013;49(6):521–543.
- 1203 [33] Sundaram, B.M., Tippur, H.V.. Dynamic fracture of soda-lime glass: A full-field optical investigation of crack initiation, propagation and
 1204 branching. *Journal of the Mechanics and Physics of Solids* 2018;120:132–153.

- 1205 [34] Bleyer, J., Roux-Langlois, C., Molinari, J.F.. Dynamic crack propagation with a variational phase-field model: limiting speed, crack
1206 branching and velocity-toughening mechanisms. *International Journal of Fracture* 2017;204(1):79–100.
- 1207 [35] Dempsey, J.P.. Dynamic crack division in brittle solids. In: *Twelfth Canadian Congress of Applied Mechanics*. 1989, p. 200–201.
- 1208 [36] Kobayashi, A., Ramulu, M.. A dynamic fracture analysis of crack curving and branching. *Le Journal de Physique Colloques*
1209 1985;46(C5):C5–197.
- 1210 [37] Kobayashi, A.. *Handbook on experimental mechanics*. Englewood Cliffs, NJ, Prentice-Hall, Inc, 1987, 1020 1987;.
- 1211 [38] Suzuki, S., Sakaue, K.. Measurement of crack opening displacement and energy release rate of rapidly bifurcating cracks in pmma by
1212 high-speed holographic microscopy. *JSME International Journal Series A Solid Mechanics and Material Engineering* 2004;47(3):264–273.
- 1213 [39] Hull, D.. *Fractography: observing, measuring and interpreting fracture surface topography*. Cambridge University Press; 1999.
- 1214 [40] Ivankovic, A., Pandya, K., Williams, J.. Crack growth predictions in polyethylene using measured traction–separation curves. *Engineering*
1215 *Fracture Mechanics* 2004;71(4-6):657–668.
- 1216 [41] Yoffe, E.H.. Lxxv. the moving griffith crack. *The London, Edinburgh, and Dublin Philosophical Magazine and Journal of Science*
1217 1951;42(330):739–750.
- 1218 [42] Broberg, K.B.. The propagation of a brittle crack. *Arkiv for Fysik* 1960;18:159–192.
- 1219 [43] Eshelby, J.. Inelastic behavior of solids. Ed Kanninen 1970;:77–115.
- 1220 [44] Gao, H.. Surface roughening and branching instabilities in dynamic fracture. *Journal of the Mechanics and Physics of Solids*
1221 1993;41(3):457–486.
- 1222 [45] Livne, A., Cohen, G., Fineberg, J.. Universality and hysteretic dynamics in rapid fracture. *Physical review letters* 2005;94(22):224301.
- 1223 [46] Adda-Bedia, M., Arias, R.. Brittle fracture dynamics with arbitrary paths i. kinking of a dynamic crack in general antiplane loading.
1224 *Journal of the Mechanics and Physics of Solids* 2003;51(7):1287–1304.
- 1225 [47] Adda-Bedia, M.. Brittle fracture dynamics with arbitrary paths. ii. dynamic crack branching under general antiplane loading. *Journal of the*
1226 *Mechanics and Physics of Solids* 2004;52(6):1407–1420.
- 1227 [48] Adda-Bedia, M.. Brittle fracture dynamics with arbitrary paths iii. the branching instability under general loading. *Journal of the Mechanics*
1228 *and Physics of Solids* 2005;53(1):227–248.
- 1229 [49] Katzav, E., Adda-Bedia, M., Arias, R.. Theory of dynamic crack branching in brittle materials. *International Journal of Fracture*
1230 2007;143(3):245–271.
- 1231 [50] Adda-Bedia, M., Arias, R.E., Bouchbinder, E., Katzav, E.. Dynamic stability of crack fronts: out-of-plane corrugations. *Physical review*
1232 *letters* 2013;110(1):014302.
- 1233 [51] Sharon, E., Cohen, G., Fineberg, J.. Crack front waves and the dynamics of a rapidly moving crack. *Physical Review Letters*
1234 2002;88(8):085503.
- 1235 [52] Bonamy, D., Ravi-Chandar, K.. Dynamic crack response to a localized shear pulse perturbation in brittle amorphous materials: on crack
1236 surface roughening. *International Journal of Fracture* 2005;134(1):1–22.
- 1237 [53] Buehler, M.J., Abraham, F.F., Gao, H.. Hyperelasticity governs dynamic fracture at a critical length scale. *Nature* 2003;426(6963):141–
1238 146.
- 1239 [54] Abraham, F.F., Gao, H.. How fast can cracks propagate? *Physical Review Letters* 2000;84(14):3113.
- 1240 [55] Gross, S.P., Fineberg, J., Marder, M., McCormick, W., Swinney, H.L.. Acoustic emissions from rapidly moving cracks. *Physical review*
1241 *letters* 1993;71(19):3162.
- 1242 [56] Linder, C., Armero, F.. Finite elements with embedded branching. *Finite Elements in Analysis and Design* 2009;45(4):280–293.
- 1243 [57] Armero, F., Linder, C.. Numerical simulation of dynamic fracture using finite elements with embedded discontinuities. *International*
1244 *Journal of Fracture* 2009;160(2):119.
- 1245 [58] Xu, D., Liu, Z., Liu, X., Zeng, Q., Zhuang, Z.. modelling of dynamic crack branching by enhanced extended finite element method.
1246 *Computational Mechanics* 2014;54(2):489–502.
- 1247 [59] Freund, L.. Crack propagation in an elastic solid subjected to general loading—i. constant rate of extension. *Journal of the Mechanics and*
1248 *Physics of Solids* 1972;20(3):129–140.
- 1249 [60] Freund, L.. Crack propagation in an elastic solid subjected to general loading—ii. non-uniform rate of extension. *Journal of the Mechanics*
1250 *and Physics of Solids* 1972;20(3):141–152.
- 1251 [61] Freund, L.. Crack propagation in an elastic solid subjected to general loading—iii. stress wave loading. *Journal of the Mechanics and*
1252 *Physics of Solids* 1973;21(2):47–61.
- 1253 [62] Clark, A., Irwin, G.. Crack-propagation behaviors. *Experimental Mechanics* 1966;6(6):321–330.
- 1254 [63] Kishen, J.C., Singh, K.D.. Stress intensity factors based fracture criteria for kinking and branching of interface crack: application to dams.
1255 *Engineering Fracture Mechanics* 2001;68(2):201–219.
- 1256 [64] Rafiee, S., Seelig, T., Gross, D.. Simulation of dynamic crack curving and branching under biaxial loading by a time domain boundary
1257 integral equation method. *International Journal of Fracture* 2003;120(3):545–561.
- 1258 [65] Zehnder, A.. *Fracture Mechanics. Lecture Notes in Applied and Computational Mechanics*; Springer Netherlands; 2012. ISBN
1259 9789400725959. URL: <https://books.google.co.uk/books?id=714J5kXbYocC>.
- 1260 [66] Tchouikov, S., Nishioka, T., Fujimoto, T.. Numerical prediction of dynamically propagating and branching cracks using moving finite
1261 element method. *CMC: Computers, Materials & Continua* 2004;1(2):191–204.
- 1262 [67] Xie, Y., Hu, X., Wang, X., Chen, J., Lee, K.. A theoretical note on mode-i crack branching and kinking. *Engineering Fracture Mechanics*
1263 2011;78(6):919–929.
- 1264 [68] Dempsey, J., Kuo, M.K., Achenbach, J.D.. Mode-iii crack kinking under stress-wave loading. *Wave Motion* 1982;4(2):181–190.
- 1265 [69] Burgers, P.. Dynamic propagation of a kinked or bifurcated crack in antiplane strain. *Journal of Applied Mechanics* 1982;49:371.
- 1266 [70] Burgers, P.. Dynamic kinking of a crack in plane strain. *International Journal of Solids and Structures* 1983;19(8):735–752.
- 1267 [71] Griffith, A.A.. Vi. the phenomena of rupture and flow in solids. *Philosophical transactions of the royal society of london Series A, containing*
1268 *papers of a mathematical or physical character* 1921;221(582-593):163–198.
- 1269 [72] Gol'dstein, R.V., Salganik, R.L.. Brittle fracture of solids with arbitrary cracks. *International journal of Fracture* 1974;10(4):507–523.

- 1270 [73] Xu, X.P., Needleman, A.. Numerical simulations of fast crack growth in brittle solids. *Journal of the Mechanics and Physics of Solids*
1271 1994;42(9):1397–1434.
- 1272 [74] Camacho, G.T., Ortiz, M.. Computational modelling of impact damage in brittle materials. *International Journal of Solids and Structures*
1273 1996;33(20-22):2899–2938.
- 1274 [75] Rabczuk, T., Belytschko, T.. Cracking particles: a simplified meshfree method for arbitrary evolving cracks. *International Journal for*
1275 *Numerical Methods in Engineering* 2004;61(13):2316–2343.
- 1276 [76] Rabczuk, T., Belytschko, T.. A three-dimensional large deformation meshfree method for arbitrary evolving cracks. *Computer methods in*
1277 *applied mechanics and engineering* 2007;196(29-30):2777–2799.
- 1278 [77] Rabczuk, T., Zi, G., Bordas, S., Nguyen-Xuan, H.. A simple and robust three-dimensional cracking-particle method without enrichment.
1279 *Computer Methods in Applied Mechanics and Engineering* 2010;199(37-40):2437–2455.
- 1280 [78] Madenci, E., Oterkus, E.. *Peridynamic theory. In: Peridynamic Theory and Its Applications*. Springer; 2014, p. 19–43.
- 1281 [79] De Borst, R.. Numerical aspects of cohesive-zone models. *Engineering fracture mechanics* 2003;70(14):1743–1757.
- 1282 [80] de Borst, R., Remmers, J.J., Needleman, A.. Mesh-independent discrete numerical representations of cohesive-zone models. *Engineering*
1283 *fracture mechanics* 2006;73(2):160–177.
- 1284 [81] Song, J.H., Wang, H., Belytschko, T.. A comparative study on finite element methods for dynamic fracture. *Computational Mechanics*
1285 2008;42(2):239–250.
- 1286 [82] Pandolfi, A., Ortiz, M.. An eigeneration approach to brittle fracture. *International Journal for Numerical Methods in Engineering*
1287 2012;92(8):694–714.
- 1288 [83] Stochino, F., Qian, A., Kaliske, M.. Eigeneration for static and dynamic brittle fracture. *Engineering Fracture Mechanics* 2017;182:537–
1289 551.
- 1290 [84] Belytschko, T., Black, T.. Elastic crack growth in finite elements with minimal remeshing. *International Journal for Numerical Methods in*
1291 *Engineering* 1999;45(5):601–620.
- 1292 [85] Moës, N., Dolbow, J., Belytschko, T.. A finite element method for crack growth without remeshing. *International Journal for Numerical*
1293 *Methods in Engineering* 1999;46(1):131–150.
- 1294 [86] Rabczuk, T., Song, J.H., Zhuang, X., Anitescu, C.. *Extended finite element and meshfree methods*. Academic Press; 2019.
- 1295 [87] Bourdin, B., Francfort, G.A., Marigo, J.J.. Numerical experiments in revisited brittle fracture. *Journal of the Mechanics and Physics of*
1296 *Solids* 2000;48(4):797–826.
- 1297 [88] Borden, M.J., Verhoosel, C.V., Scott, M.A., Hughes, T.J., Landis, C.M.. A phase-field description of dynamic brittle fracture. *Computer*
1298 *Methods in Applied Mechanics and Engineering* 2012;217:77–95.
- 1299 [89] Bažant, Z.P., Jirásek, M.. Nonlocal integral formulations of plasticity and damage: survey of progress. *Journal of engineering mechanics*
1300 2002;128(11):1119–1149.
- 1301 [90] Friedman, J., Popescu, B.E.. Gradient directed regularization for linear regression and classification. Tech. Rep.; Technical Report,
1302 Statistics Department, Stanford University; 2003.
- 1303 [91] Rabczuk, T.. Computational methods for fracture in brittle and quasi-brittle solids: state-of-the-art review and future perspectives. *ISRN*
1304 *Applied Mathematics* 2013;2013.
- 1305 [92] Mohammadnejad, M., Liu, H., Chan, A., Dehkoda, S., Fukuda, D.. An overview on advances in computational fracture mechanics of
1306 rock. *Geosystem Engineering* 2018;:1–24.
- 1307 [93] Jung, J., Yang, Q.. A two-dimensional augmented finite element for dynamic crack initiation and propagation. *International Journal of*
1308 *Fracture* 2017;203(1-2):41–61.
- 1309 [94] Schmidt, B., Fraternali, F., Ortiz, M.. Eigenfracture: an eigendeformation approach to variational fracture. *Multiscale Modeling &*
1310 *Simulation* 2009;7(3):1237–1266.
- 1311 [95] Fan, Z., Liao, H., Jiang, H., Wang, H., Li, B.. A dynamic adaptive eigenfracture method for failure in brittle materials. *Engineering*
1312 *Fracture Mechanics* 2021;244:107540.
- 1313 [96] Fries, T.P., Belytschko, T.. The extended/generalized finite element method: an overview of the method and its applications. *International*
1314 *journal for numerical methods in engineering* 2010;84(3):253–304.
- 1315 [97] Rabczuk, T., Zi, G.. A meshfree method based on the local partition of unity for cohesive cracks. *Computational Mechanics*
1316 2007;39(6):743–760.
- 1317 [98] Rabczuk, T., Song, J.H., Belytschko, T.. Simulations of instability in dynamic fracture by the cracking particles method. *Engineering*
1318 *Fracture Mechanics* 2009;76(6):730–741.
- 1319 [99] Ai, W., Augarde, C.E.. An adaptive cracking particle method for 2d crack propagation. *International journal for numerical methods in*
1320 *engineering* 2016;108(13):1626–1648.
- 1321 [100] Ai, W., Augarde, C.E.. A multi-cracked particle method for complex fracture problems in 2d. *Mathematics and Computers in Simulation*
1322 2018;150:1–24.
- 1323 [101] Xu, S.. Stable cracking particles method based on stabilized nodal integration and updated lagrangian kernel. *Mathematical Problems in*
1324 *Engineering* 2014;2014.
- 1325 [102] Dugdale, D.S.. Yielding of steel sheets containing slits. *Journal of the Mechanics and Physics of Solids* 1960;8(2):100–104.
- 1326 [103] Barenblatt, G.I.. *The mathematical theory of equilibrium cracks in brittle fracture*; vol. 7. Elsevier; 1962.
- 1327 [104] Needleman, A.. A continuum model for void nucleation by inclusion debonding. *Journal of Applied Mechanics* 1987;54(3):525–531.
- 1328 [105] Geubelle, P.H., Baylor, J.S.. Impact-induced delamination of composites: a 2d simulation. *Composites Part B: Engineering*
1329 1998;29(5):589–602.
- 1330 [106] Pandolfi, A., Ortiz, M.. An efficient adaptive procedure for three-dimensional fragmentation simulations. *Engineering with Computers*
1331 2002;18(2):148–159.
- 1332 [107] Park, K., Paulino, G.H.. Cohesive zone models: a critical review of traction-separation relationships across fracture surfaces. *Applied*
1333 *Mechanics Reviews* 2011;64(6).
- 1334 [108] Seagraves, A., Radovitzky, R.. Advances in cohesive zone modeling of dynamic fracture. In: *Dynamic failure of materials and structures*.

- Springer; 2009, p. 349–405.
- [109] Papoulia, K.D., Sam, C.H., Vavasis, S.A.. Time continuity in cohesive finite element modelling. *International Journal for Numerical Methods in Engineering* 2003;58(5):679–701.
- [110] Radovitzky, R., Seagraves, A., Tupek, M., Noels, L.. A scalable 3d fracture and fragmentation algorithm based on a hybrid, discontinuous galerkin, cohesive element method. *Computer Methods in Applied Mechanics and Engineering* 2011;200(1-4):326–344.
- [111] Sam, C.H., Papoulia, K.D., Vavasis, S.A.. Obtaining initially rigid cohesive finite element models that are temporally convergent. *Engineering Fracture Mechanics* 2005;72(14):2247–2267.
- [112] Arias, I., Knap, J., Chalivendra, V.B., Hong, S., Ortiz, M., Rosakis, A.J.. Numerical modelling and experimental validation of dynamic fracture events along weak planes. *Computer Methods in Applied Mechanics and Engineering* 2007;196(37-40):3833–3840.
- [113] Agwai, A., Guven, I., Madenci, E.. Predicting crack propagation with peridynamics: a comparative study. *International Journal of Fracture* 2011;171(1):65.
- [114] Paulino, G.H., Park, K., Celes, W., Espinha, R.. Adaptive dynamic cohesive fracture simulation using nodal perturbation and edge-swap operators. *International Journal for Numerical Methods in Engineering* 2010;84(11):1303–1343.
- [115] Leon, S., Spring, D., Paulino, G.. Reduction in mesh bias for dynamic fracture using adaptive splitting of polygonal finite elements. *International Journal for Numerical Methods in Engineering* 2014;100(8):555–576.
- [116] Spring, D.W., Leon, S.E., Paulino, G.H.. Unstructured polygonal meshes with adaptive refinement for the numerical simulation of dynamic cohesive fracture. *International Journal of Fracture* 2014;189(1):33–57.
- [117] Choi, H., Park, K.. Removing mesh bias in mixed-mode cohesive fracture simulation with stress recovery and domain integral. *International Journal for Numerical Methods in Engineering* 2019;120(9):1047–1070.
- [118] Zhang, Z., Paulino, G.H., Celes, W.. Extrinsic cohesive modelling of dynamic fracture and microbranching instability in brittle materials. *International Journal for Numerical Methods in Engineering* 2007;72(8):893–923.
- [119] Miller, O., Freund, L., Needleman, A.. Energy dissipation in dynamic fracture of brittle materials. *Modelling and Simulation in Materials Science and Engineering* 1999;7(4):573.
- [120] Park, K., Paulino, G.H., Celes, W., Espinha, R.. Adaptive mesh refinement and coarsening for cohesive zone modelling of dynamic fracture. *International Journal for Numerical Methods in Engineering* 2012;92(1):1–35.
- [121] Nguyen, V.P.. Discontinuous galerkin/extrinsic cohesive zone modelling: Implementation caveats and applications in computational fracture mechanics. *Engineering Fracture Mechanics* 2014;128:37–68.
- [122] Becker, G., Noels, L.. A full-discontinuous galerkin formulation of nonlinear kirchhoff–love shells: elasto-plastic finite deformations, parallel computation, and fracture applications. *International Journal for Numerical Methods in Engineering* 2013;93(1):80–117.
- [123] Baek, H., Kweon, C., Park, K.. Multiscale dynamic fracture analysis of composite materials using adaptive microstructure modeling. *International Journal for Numerical Methods in Engineering* 2020;121(24):5719–5741.
- [124] Park, K., Paulino, G.H., Roesler, J.R.. A unified potential-based cohesive model of mixed-mode fracture. *Journal of the Mechanics and Physics of Solids* 2009;57(6):891–908.
- [125] Park, K., Paulino, G.H.. Computational implementation of the ppr potential-based cohesive model in abaqus: Educational perspective. *Engineering fracture mechanics* 2012;93:239–262.
- [126] Park, K., Choi, H., Paulino, G.H.. Assessment of cohesive traction-separation relationships in abaqus: A comparative study. *Mechanics Research Communications* 2016;78:71–78.
- [127] Baek, H., Park, K.. Cohesive frictional-contact model for dynamic fracture simulations under compression. *International Journal of Solids and Structures* 2018;144:86–99.
- [128] Abedi, R., Haber, R.B., Clarke, P.L.. Effect of random defects on dynamic fracture in quasi-brittle materials. *International Journal of Fracture* 2017;208(1):241–268.
- [129] Francfort, G.A., Marigo, J.J.. Revisiting brittle fracture as an energy minimization problem. *Journal of the Mechanics and Physics of Solids* 1998;46(8):1319–1342.
- [130] Chen, B., Sun, Y., Barboza, B.R., Barron, A.R., Li, C.. Phase-field simulation of hydraulic fracturing with a revised fluid model and hybrid solver. *Engineering Fracture Mechanics* 2020;229:106928.
- [131] Hofacker, M., Miehe, C.. Continuum phase field modeling of dynamic fracture: variational principles and staggered fe implementation. *International Journal of Fracture* 2012;178(1-2):113–129.
- [132] Bleyer, J., Molinari, J.F.. Microbranching instability in phase-field modelling of dynamic brittle fracture. *Applied Physics Letters* 2017;110(15):151903.
- [133] Wu, J.Y., Nguyen, V.P.. A length scale insensitive phase-field damage model for brittle fracture. *Journal of the Mechanics and Physics of Solids* 2018;119:20–42.
- [134] Wu, J.Y.. A unified phase-field theory for the mechanics of damage and quasi-brittle failure. *Journal of the Mechanics and Physics of Solids* 2017;103:72–99.
- [135] Nguyen, V.P., Wu, J.Y.. Modeling dynamic fracture of solids with a phase-field regularized cohesive zone model. *Computer Methods in Applied Mechanics and Engineering* 2018;340:1000–1022.
- [136] Zhou, S., Zhuang, X., Zhu, H., Rabczuk, T.. Phase field modelling of crack propagation, branching and coalescence in rocks. *Theoretical and Applied Fracture Mechanics* 2018;96:174–192.
- [137] Zhou, S., Zhuang, X., Rabczuk, T.. Phase-field modelling of fluid-driven dynamic cracking in porous media. *Computer Methods in Applied Mechanics and Engineering* 2019;.
- [138] Ren, H., Zhuang, X., Anitescu, C., Rabczuk, T.. An explicit phase field method for brittle dynamic fracture. *Computers & Structures* 2019;217:45–56.
- [139] Wu, J.Y., Nguyen, V.P., Nguyen, C.T., Sutula, D., Bordas, S., Sinaie, S.. Phase field modeling of fracture. *Advances in Applied mechanics: Multi-scale Theory and Computation* 2018;52.
- [140] Hofacker, M., Miehe, C.. A phase field model of dynamic fracture: Robust field updates for the analysis of complex crack patterns. *International Journal for Numerical Methods in Engineering* 2013;93(3):276–301.

- [141] Henry, H. Study of the branching instability using a phase field model of inplane crack propagation. *EPL (Europhysics Letters)* 2008;83(1):16004.
- [142] Tian, F., Tang, X., Xu, T., Yang, J., Li, L.. Bifurcation criterion and the origin of limit crack velocity in dynamic brittle fracture. *International Journal of Fracture* 2020;224:117–131.
- [143] Mandal, T.K., Nguyen, V.P., Wu, J.Y.. Evaluation of variational phase-field models for dynamic brittle fracture. *Engineering Fracture Mechanics* 2020;235:107169.
- [144] Dinachandra, M., Alankar, A.. A phase-field study of crack propagation and branching in functionally graded materials using explicit dynamics. *Theoretical and Applied Fracture Mechanics* 2020;109:102681.
- [145] Kamensky, D., Moutsanidis, G., Bazilevs, Y.. Hyperbolic phase field modeling of brittle fracture: part i—theory and simulations. *Journal of the Mechanics and Physics of Solids* 2018;121:81–98.
- [146] Liu, G., Li, Q., Msekh, M.A., Zuo, Z.. Abaqus implementation of monolithic and staggered schemes for quasi-static and dynamic fracture phase-field model. *Computational Materials Science* 2016;121:35–47.
- [147] Zhou, S., Rabczuk, T., Zhuang, X.. Phase field modeling of quasi-static and dynamic crack propagation: Comsol implementation and case studies. *Advances in Engineering Software* 2018;122:31–49.
- [148] Steinke, C., Özenç, K., Chinaryan, G., Kaliske, M.. A comparative study of the r-adaptive material force approach and the phase-field method in dynamic fracture. *International Journal of Fracture* 2016;201(1):97–118.
- [149] Jirasek, M.. Nonlocal models for damage and fracture: comparison of approaches. *International Journal of Solids and Structures* 1998;35(31-32):4133–4145.
- [150] Karihaloo, B.. Failure of concrete. In: Milne, I., Ritchie, R., Karihaloo, B., editors. *Comprehensive Structural Integrity*. Oxford: Pergamon. ISBN 978-0-08-043749-1; 2003, p. 477–548. doi:<https://doi.org/10.1016/B0-08-043749-4/02087-5>.
- [151] Wolff, C., Richart, N., Molinari, J.F.. A non-local continuum damage approach to model dynamic crack branching. *International Journal for Numerical Methods in Engineering* 2015;101(12):933–949.
- [152] Wang, Z., Shedbale, A.S., Kumar, S., Poh, L.H.. Localizing gradient damage model with micro inertia effect for dynamic fracture. *Computer Methods in Applied Mechanics and Engineering* 2019;355:492–512.
- [153] Milne, I., Ritchie, R.O., Karihaloo, B.L.. *Comprehensive structural integrity: Cyclic loading and fatigue*; vol. 4. Elsevier; 2003.
- [154] Pradhan, K.K., Chakraverty, S.. Chapter four - finite element method. In: Pradhan, K.K., Chakraverty, S., editors. *Computational Structural Mechanics*. Academic Press. ISBN 978-0-12-815492-2; 2019, p. 25–28. doi:<https://doi.org/10.1016/B978-0-12-815492-2.00010-1>.
- [155] Chen, B., Cen, S., Barron, A.R., Owen, D., Li, C.. Numerical investigation of the fluid lag during hydraulic fracturing. *Engineering Computations* 2018;35(5):2050–2077.
- [156] Newmark, N.M.. A method of computation for structural dynamics. *Journal of the Engineering Mechanics Division* 1959;85(3):67–94.
- [157] Zhuang, Z., Liu, Z., Cheng, B., Liao, J.. *Extended Finite Element Method: Tsinghua University Press Computational Mechanics Series*. Tsinghua University Press Computational Mechanics; Elsevier Science; 2014.
- [158] Gupta, V., Duarte, C.A., Babuška, I., Banerjee, U.. A stable and optimally convergent generalized fem (sgfem) for linear elastic fracture mechanics. *Computer methods in applied mechanics and engineering* 2013;266:23–39.
- [159] Gupta, V., Duarte, C., Babuška, I., Banerjee, U.. Stable gfem (sgfem): Improved conditioning and accuracy of gfem/xfem for three-dimensional fracture mechanics. *Computer methods in applied mechanics and engineering* 2015;289:355–386.
- [160] Wu, J.Y., Li, F.B.. An improved stable xfem (is-xfem) with a novel enrichment function for the computational modeling of cohesive cracks. *Computer Methods in Applied Mechanics and Engineering* 2015;295:77–107.
- [161] Khoei, A.. *Extended Finite Element Method: Theory and Applications*. Wiley Series in Computational Mechanics; Wiley; 2015. ISBN 9781118457689. URL: <https://books.google.co.uk/books?id=unKwCQAAQBAJ>.
- [162] Daux, C., Moës, N., Dolbow, J., Sukumar, N., Belytschko, T.. Arbitrary branched and intersecting cracks with the extended finite element method. *International Journal for Numerical Methods in Engineering* 2000;48(12):1741–1760.
- [163] Belytschko, T., Chen, H., Xu, J., Zi, G.. Dynamic crack propagation based on loss of hyperbolicity and a new discontinuous enrichment. *International journal for numerical methods in engineering* 2003;58(12):1873–1905.
- [164] Chen, J.W., Zhou, X.P.. The enhanced extended finite element method for the propagation of complex branched cracks. *Engineering Analysis with Boundary Elements* 2019;104:46–62.
- [165] Song, J.H., Areias, P.M., Belytschko, T.. A method for dynamic crack and shear band propagation with phantom nodes. *International Journal for Numerical Methods in Engineering* 2006;67(6):868–893.
- [166] Song, J.H., Belytschko, T.. Cracking node method for dynamic fracture with finite elements. *International Journal for Numerical Methods in Engineering* 2009;77(3):360–385.
- [167] Aliabadi, M.H.. *Boundary Element Methods in Linear Elastic Fracture Mechanics*. Elsevier; 2016.
- [168] Liu, Y., Mukherjee, S., Nishimura, N., Schanz, M., Ye, W., Sutradhar, A., et al. Recent advances and emerging applications of the boundary element method. *Applied Mechanics Reviews* 2011;64(3).
- [169] Seelig, T., Gross, D.. On the interaction and branching of fast running cracks—a numerical investigation. *Journal of the Mechanics and Physics of Solids* 1999;47(4):935–952.
- [170] Rajapakse, R., Xu, X.L.. Boundary element modelling of cracks in piezoelectric solids. *Engineering Analysis with Boundary Elements* 2001;25(9):771–781.
- [171] Yan, X.. Numerical analysis of a few complex crack problems with a boundary element method. *Engineering Failure Analysis* 2006;13(5):805–825.
- [172] Marji, M.F.. Numerical analysis of quasi-static crack branching in brittle solids by a modified displacement discontinuity method. *International Journal of Solids and Structures* 2014;51(9):1716–1736.
- [173] Santana, E., Portela, A.. Dual boundary element analysis of fatigue crack growth, interaction and linkup. *Engineering Analysis with Boundary Elements* 2016;64:176–195.
- [174] Fedelinski, P.. Dynamically loaded branched and intersecting cracks. *Czasopismo Inzynierii Ladowej, Srodowiska i Architektury* 2017;.

- 1465 [175] Shrivastava, K., Sharma, M.M., et al. Mechanisms for the formation of complex fracture networks in naturally fractured rocks. 2018.
- 1466 [176] Nguyen, V.P., Rabczuk, T., Bordas, S., Duflo, M.. Meshless methods: a review and computer implementation aspects. *Mathematics and*
1467 *computers in simulation* 2008;79(3):763–813.
- 1468 [177] Wang, H., Qin, Q.H.. *Methods of fundamental solutions in solid mechanics*. Elsevier; 2019.
- 1469 [178] Gingold, R.A., Monaghan, J.J.. Smoothed particle hydrodynamics: theory and application to non-spherical stars. *Monthly notices of the*
1470 *royal astronomical society* 1977;181(3):375–389.
- 1471 [179] Liu, G.R., Gu, Y.T.. *An introduction to meshfree methods and their programming*. Springer Science & Business Media; 2005.
- 1472 [180] Zhuang, X., Augarde, C., Mathisen, K.. Fracture modeling using meshless methods and level sets in 3d: framework and modeling.
1473 *International Journal for Numerical Methods in Engineering* 2012;92(11):969–998.
- 1474 [181] Huerta, A., Belytschko, T., Fernández-Méndez, S., Rabczuk, T., Zhuang, X., Arroyo, M.. Meshfree methods. *Encyclopedia of*
1475 *Computational Mechanics Second Edition* 2018;:1–38.
- 1476 [182] Monaghan, J.J., Gingold, R.A.. Shock simulation by the particle method sph. *Journal of computational physics* 1983;52(2):374–389.
- 1477 [183] Libersky, L.D., Petschek, A.G., Carney, T.C., Hipp, J.R., Allahdadi, F.A.. High strain lagrangian hydrodynamics: a three-dimensional
1478 sph code for dynamic material response. *Journal of computational physics* 1993;109(1):67–75.
- 1479 [184] Libersky, L.D., Randles, P.W., Carney, T.C., Dickinson, D.L.. Recent improvements in sph modeling of hypervelocity impact. *Internation-*
1480 *al Journal of Impact Engineering* 1997;20(6-10):525–532.
- 1481 [185] Randles, P., Libersky, L.D.. Smoothed particle hydrodynamics: some recent improvements and applications. *Computer methods in applied*
1482 *mechanics and engineering* 1996;139(1-4):375–408.
- 1483 [186] Rabczuk, T., Eibl, J.. Simulation of high velocity concrete fragmentation using sph/mlsph. *International Journal for Numerical Methods in*
1484 *Engineering* 2003;56(10):1421–1444.
- 1485 [187] Rabczuk, T., Eibl, J.. Modelling dynamic failure of concrete with meshfree methods. *International Journal of Impact Engineering*
1486 *2006;32(11):1878–1897*.
- 1487 [188] Rajagopal, S., Gupta, N.. Meshfree modelling of fracture—a comparative study of different methods. *Meccanica* 2011;46(5):1145–1158.
- 1488 [189] Rabczuk, T., Belytschko, T., Xiao, S.. Stable particle methods based on lagrangian kernels. *Computer methods in applied mechanics and*
1489 *engineering* 2004;193(12-14):1035–1063.
- 1490 [190] Vignjevic, R., Reveles, J.R., Campbell, J.. Sph in a total lagrangian formalism. *CMC-Tech Science Press-* 2006;4(3):181.
- 1491 [191] Chakraborty, S., Shaw, A.. A pseudo-spring based fracture model for sph simulation of impact dynamics. *International Journal of Impact*
1492 *Engineering* 2013;58:84–95.
- 1493 [192] Islam, M.R.I., Shaw, A.. Numerical modelling of crack initiation, propagation and branching under dynamic loading. *Engineering Fracture*
1494 *Mechanics* 2020;224:106760.
- 1495 [193] Belytschko, T., Lu, Y.Y., Gu, L.. Element-free galerkin methods. *International journal for numerical methods in engineering*
1496 *1994;37(2):229–256*.
- 1497 [194] Rabczuk, T., Areias, P.. A meshfree thin shell for arbitrary evolving cracks based on an extrinsic basis. *Computer mechanics* 2006;.
- 1498 [195] Zi, G., Rabczuk, T., Wall, W.. Extended meshfree methods without branch enrichment for cohesive cracks. *Computational Mechanics*
1499 *2007;40(2):367–382*.
- 1500 [196] Bordas, S., Rabczuk, T., Zi, G.. Three-dimensional crack initiation, propagation, branching and junction in non-linear materials by an
1501 extended meshfree method without asymptotic enrichment. *Engineering Fracture Mechanics* 2008;75(5):943–960.
- 1502 [197] Rabczuk, T., Bordas, S., Zi, G.. On three-dimensional modelling of crack growth using partition of unity methods. *Computers & structures*
1503 *2010;88(23-24):1391–1411*.
- 1504 [198] Liu, W.K., Jun, S., Zhang, Y.F.. Reproducing kernel particle methods. *International journal for numerical methods in fluids* 1995;20(8-
1505 *9):1081–1106*.
- 1506 [199] Guan, P.C., Chi, S., Chen, J., Slawson, T., Roth, M.. Semi-lagrangian reproducing kernel particle method for fragment-impact problems.
1507 *International Journal of Impact Engineering* 2011;38(12):1033–1047.
- 1508 [200] Klein, P., Foulk, J., Chen, E., Wimmer, S., Gao, H.. Physics-based modelling of brittle fracture: cohesive formulations and the application
1509 of meshfree methods. *Theoretical and Applied Fracture Mechanics* 2001;37(1-3):99–166.
- 1510 [201] Sulsky, D., Chen, Z., Schreyer, H.L.. A particle method for history-dependent materials. *Computer methods in applied mechanics and*
1511 *engineering* 1994;118(1-2):179–196.
- 1512 [202] Li, S., Zhang, Y., Wu, J., Yu, J., Gong, X.. Modeling of crack propagation with the quasi-static material point method. *Engineering*
1513 *Fracture Mechanics* 2021;245:107602.
- 1514 [203] Ma, S., Zhang, X.. Material point method for impact and explosion problems. In: *Computational Mechanics*. Springer; 2007, p. 156–166.
- 1515 [204] Schreyer, H., Sulsky, D., Zhou, S.J.. Modeling delamination as a strong discontinuity with the material point method. *Computer Methods*
1516 *in Applied Mechanics and Engineering* 2002;191(23-24):2483–2507.
- 1517 [205] Nairn, J.A.. Material point method calculations with explicit cracks. *Computer Modeling in Engineering and Sciences* 2003;4(6):649–664.
- 1518 [206] Liang, Y., Benedek, T., Zhang, X., Liu, Y.. Material point method with enriched shape function for crack problems. *Computer Methods*
1519 *in Applied Mechanics and Engineering* 2017;322:541–562.
- 1520 [207] Daphalapurkar, N.P., Lu, H., Coker, D., Komanduri, R.. Simulation of dynamic crack growth using the generalized interpolation material
1521 point (gimp) method. *International Journal of Fracture* 2007;143(1):79–102.
- 1522 [208] Kakouris, E.G., Triantafyllou, S.P.. Phase-field material point method for dynamic brittle fracture with isotropic and anisotropic surface
1523 energy. *Computer Methods in Applied Mechanics and Engineering* 2019;357:112503.
- 1524 [209] Silling, S.A.. Reformulation of elasticity theory for discontinuities and long-range forces. *Journal of the Mechanics and Physics of Solids*
1525 *2000;48(1):175–209*.
- 1526 [210] Silling, S.A., Epton, M., Weckner, O., Xu, J., Askari, E.. Peridynamic states and constitutive modelling. *Journal of Elasticity*
1527 *2007;88(2):151–184*.
- 1528 [211] Ren, H., Zhuang, X., Cai, Y., Rabczuk, T.. Dual-horizon peridynamics. *International Journal for Numerical Methods in Engineering*
1529 *2016;108(12):1451–1476*.

- 1530 [212] Ren, H., Zhuang, X., Rabczuk, T. Dual-horizon peridynamics: A stable solution to varying horizons. *Computer Methods in Applied*
1531 *Mechanics and Engineering* 2017;318:762–782.
- 1532 [213] Rabczuk, T., Ren, H.. A peridynamics formulation for quasi-static fracture and contact in rock. *Engineering Geology* 2017;225:42–48.
- 1533 [214] Zhou, X., Wang, Y., Qian, Q.. Numerical simulation of crack curving and branching in brittle materials under dynamic loads using the
1534 extended non-ordinary state-based peridynamics. *European Journal of Mechanics-A/Solids* 2016;60:277–299.
- 1535 [215] Dipasquale, D., Zaccariotto, M., Galvanetto, U.. Crack propagation with adaptive grid refinement in 2d peridynamics. *International*
1536 *Journal of Fracture* 2014;190(1-2):1–22.
- 1537 [216] Ha, Y.D., Bobaru, F.. Studies of dynamic crack propagation and crack branching with peridynamics. *International Journal of Fracture*
1538 2010;162(1-2):229–244.
- 1539 [217] Ha, Y.D., Bobaru, F.. Characteristics of dynamic brittle fracture captured with peridynamics. *Engineering Fracture Mechanics*
1540 2011;78(6):1156–1168.
- 1541 [218] Bobaru, F., Zhang, G.. Why do cracks branch? a peridynamic investigation of dynamic brittle fracture. *International Journal of Fracture*
1542 2015;196(1-2):59–98.
- 1543 [219] Butt, S.N., Meschke, G.. Peridynamic analysis of dynamic fracture: influence of peridynamic horizon, dimensionality and specimen size.
1544 *Computational Mechanics* 2021;67(6):1719–1745.
- 1545 [220] Bobaru, F., Hu, W.. The meaning, selection, and use of the peridynamic horizon and its relation to crack branching in brittle materials.
1546 *International Journal of Fracture* 2012;176(2):215–222.
- 1547 [221] Chen, Z., Ju, J.W., Su, G., Huang, X., Li, S., Zhai, L.. Influence of micro-modulus functions on peridynamics simulation of crack
1548 propagation and branching in brittle materials. *Engineering Fracture Mechanics* 2019;216:106498.
- 1549 [222] Cundall, P.A., Strack, O.D.. A discrete numerical model for granular assemblies. *Geotechnique* 1979;29(1):47–65.
- 1550 [223] Jing, L., Stephansson, O.. *Fundamentals of discrete element methods for rock engineering: theory and applications*. Elsevier; 2007.
- 1551 [224] Hedjazi, L., Martin, C., Guessasma, S., Della Valle, G., Dendievel, R.. Application of the discrete element method to crack propagation
1552 and crack branching in a vitreous dense biopolymer material. *International Journal of Solids and Structures* 2012;49(13):1893–1899.
- 1553 [225] Lisjak, A., Grasselli, G.. A review of discrete modelling techniques for fracturing processes in discontinuous rock masses. *Journal of Rock*
1554 *Mechanics and Geotechnical Engineering* 2014;6(4):301–314.
- 1555 [226] Leclerc, W., Haddad, H., Guessasma, M.. On the suitability of a discrete element method to simulate cracks initiation and propagation in
1556 heterogeneous media. *International Journal of Solids and Structures* 2017;108:98–114.
- 1557 [227] Hofmann, H., Babadagli, T., Zimmermann, G.. A grain based modelling study of fracture branching during compression tests in granites.
1558 *International Journal of Rock Mechanics and Mining Sciences* 2015;77:152–162.
- 1559 [228] Chung, Y., Yang, Z., Lin, C.. Modelling micro-crack initiation and propagation of crystal structures with microscopic defects under
1560 uni-axial tension by discrete element method. *Powder Technology* 2017;315:445–476.